EFFICIENT COMPUTATION OF THE GREEN'S FUNCTION FOR MULTILAYER STRUCTURES WITH PERIODIC DIELECTRIC GRATINGS

A THESIS SUBMITTED TO
THE GRADUATE SCHOOL OF NATURAL AND APPLIED SCIENCES
OF
MIDDLE EAST TECHNICAL UNIVERSITY

BY

SÜLEYMAN ADANIR

IN PARTIAL FULFILLMENT OF THE REQUIREMENTS
FOR
THE DEGREE OF MASTER OF SCIENCE
IN
ELECTRICAL AND ELECTRONICS ENGINEERING

FEBRUARY 2011

Approval of the thesis:

EFFICIENT COMPUTATION OF THE GREEN'S FUNCTION FOR MULTILAYER STRUCTURES WITH PERIODIC DIELECTRIC GRATINGS

submitted by **SÜLEYMAN ADANIR** in partial fulfillment of the requirements for the degree of **Master of Science in Electrical and Electronics Engineering Department, Middle East Technical University** by,

Prof. Dr. Canan Özgen _____
Dean, Graduate School of **Natural and Applied Sciences**

Prof. Dr. İsmet Erkmen _____
Head of Department, **Electrical and Electronics Engineering**

Assoc. Prof. Dr. Lale Alatan _____
Supervisor, **Electrical and Electronics Engineering Dept., METU**

Examining Committee Members:

Prof. Dr. Gülbin Dural
Electrical and Electronics Engineering Dept., METU _____

Assoc. Prof. Dr. Lale Alatan
Electrical and Electronics Engineering Dept., METU _____

Prof. Dr. Sencer Koç
Electrical and Electronics Engineering Dept., METU _____

Prof. Dr. Özlem Aydın Çivi
Electrical and Electronics Engineering Dept., METU _____

Assoc. Prof. Dr. Vakur B. Ertürk
Electrical and Electronics Engineering Dept., Bilkent University _____

Date: _____

I hereby declare that all information in this document has been obtained and presented in accordance with academic rules and ethical conduct. I also declare that, as required by these rules and conduct, I have fully cited and referenced all material and results that are not original to this work.

Name, Last Name: SÜLEYMAN ADANIR

Signature :

ABSTRACT

EFFICIENT COMPUTATION OF THE GREEN'S FUNCTION FOR MULTILAYER STRUCTURES WITH PERIODIC DIELECTRIC GRATINGS

Adanır, Süleyman
M.Sc., Department of Electrical and Electronics Engineering
Supervisor : Assoc. Prof. Dr. Lale Alatan

February 2011, 57 pages

Numerical analysis of periodic structures in layered media is usually accomplished by using Method of Moments which requires the formation of the impedance matrix of the structure. The construction of this impedance matrix requires the evaluation of the periodic Green's function in layered media which is expressed as an infinite series in terms of the spectral domain Green's function. The slow converging nature of this series make these kinds of analysis computationally expensive. Although some papers have proposed methods to accelerate the computation of these series successfully for a single frequency point, it is still very computation intensive to obtain the frequency response of the structure over a band of frequencies. In this thesis, Discrete Complex Image Method (DCIM) is utilized for the efficient computation of the periodic Green's function. First, the spectral domain Green's function in layered media is approximated by complex exponentials through the use of DCIM. During the application of the DCIM, three-level approximation scheme is employed to improve accuracy. Then, Ewald's transformation is applied to accelerate the computation of the infinite series involved in the periodic Green's functions. The accuracy and the efficiency of the method is demonstrated through numerical examples.

Keywords: Multilayer media, periodic structures, Green's function, complex images, Ewald Method

ÖZ

PERİYODİK OLARAK DİELEKTRİK AÇIKLIK BIRAKILMIŞ ÇOK KATMANLI YAPILARIN GREEN FONKSİYONUNUN İŞLEMSEL OLARAK VERİMLİ BİR ŞEKİLDE HESAPLANMASI

Adanır, Süleyman
Yüksek Lisans, Elektrik ve Elektronik Mühendisliği Bölümü
Tez Yöneticisi : Doç. Dr. Lale Alatan

Şubat 2011, 57 sayfa

Çok katmanlı ortamlardaki periyodik yapıların sayısal analizi çoğunlukla yapının empedans matrisine ihtiyaç duyan MoM ile yapılır. Bu empedans matrisinin oluşturulması için de Green fonksiyonunun hesaplanması gerekmektedir. Bu tür yapılardaki Green fonksiyonunun yakınsama hızı düşük olan sonsuz bir seri olarak ifade edilmesi bu yapıların analizinin çok süre almasına sebep olur. Bu seriyi bir frekansta başarılı bir şekilde hızlandırmak için yöntemler öneren yayınlar çıkmış olmasına rağmen, yapının bir bant boyunca frekans yanıtını elde etmek hala uzun süren bir işlem olarak kalmaktadır. Periyodik Green fonksiyonunun verimli olarak hesaplanabilmesi için Ayrık Karmaşık İmgeler Metodu'ndan (DCIM) faydalanılmıştır. Önce, çok katmanlı yapının spektral uzaydaki Green fonksiyonu DCIM kullanılarak, karmaşık üstellerle yaklaştırılmıştır. DCIM metodu uygulanırken doğruluğu iyileştirmek amacıyla üç-seviyeli yaklaştırma yöntemi kullanılmıştır. Daha sonra, periyodik Green fonksiyonlarının içerdiği sonsuz serilerin hesaplanmasını hızlandırmak için Ewald dönüşümü uygulanmıştır. Yöntemin doğruluğu ve verimliliği sayısal örneklerle gösterilmiştir.

Anahtar Kelimeler: Çok katmanlı ortamlar, periyodik yapılar, Green fonksiyonu, karmaşık imgeler, Ewald Yöntemi

to my family

ACKNOWLEDGMENTS

I would like to express my gratitude and deep appreciation to my supervisor Assoc. Prof. Dr. Lale Alatan for her guidance, support and valuable recommendations throughout my thesis work.

I am also grateful to Aselsan Electronics Industries Inc. for its support to my graduate study and to TÜBİTAK for its financial support offered during this study. I also would like to thank my colleagues in Aselsan for their understanding in my hard times.

Finally, I would like to express my deep appreciation to my family for their confidence and endless support which helped me to accomplish this work.

TABLE OF CONTENTS

ABSTRACT iv

ÖZ vi

ACKNOWLEDGMENTS ix

TABLE OF CONTENTS x

LIST OF TABLES xii

LIST OF FIGURES xiii

CHAPTERS

1 INTRODUCTION 1

2 BACKGROUND INFORMATION 6

2.1 Discrete Complex Image Method 6

2.2 Surface Wave Poles 14

2.3 Ewald's Transformation 17

3 NUMERICAL RESULTS FOR THE COMPUTATION OF THE PERIODIC GREEN'S FUNCTION IN LAYERED MEDIA 22

3.1 Two-Level Discrete Complex Image Method 24

3.1.1 Formulation 24

3.1.2 Numerical Results 26

3.2 Two-Level Discrete Complex Image Method with Surface Wave Pole Extraction 30

3.2.1 Formulation 30

3.2.2 Numerical Results 31

3.3 Three-Level Discrete Complex Image Method with Surface Wave Pole Extraction 34

3.3.1 Formulation 34

3.3.2 Numerical Results 36

4 ACCELERATING THE COMPUTATION OF THE SERIES REPRESENTING THE PERIODIC GREEN'S FUNCTION IN LAYERED MEDIA 40

4.1 Formulation 40

4.2 Numerical Results 43

5 CONCLUSION AND THE FUTURE WORK 52

REFERENCES 54

LIST OF TABLES

TABLES

Table 3.1 The parameters of the structure used during the simulations 27

Table 3.2 Approximation parameters of the 2-Level DCIM 27

Table 3.3 Approximation parameters for 2-Level DCIM with SW Extraction Approach 31

Table 3.4 Approximation parameters for 3-Level DCIM Approach 36

LIST OF FIGURES

FIGURES

Figure 1.1 Periodic structure with dielectric gratings [8] 1

Figure 1.2 Example of a periodic structure with conducting patches (a 2-D mushroom type left-handed material) [5] 2

Figure 2.1 Sommerfeld Integration Path 7

Figure 2.2 The sampling paths on the complex: (a) k_ρ plane and (b) k_{z0} plane [21] . . 9

Figure 2.3 The sampling path on the complex k_ρ plane in [24] 10

Figure 2.4 Path for the first 3-level DCIM approach on the complex: (a) k_z plane and (b) k_ρ plane [27] 12

Figure 2.5 Path for the second 3-level DCIM approach on the complex: (a) k_z plane and (b) k_ρ plane [27] 13

Figure 2.6 Path for the third 3-level DCIM approach on the complex: (a) k_ρ plane and (b) k_z plane [27] 14

Figure 2.7 Path of integration for the case $\alpha_k \in [0, \pi/2]$ 19

Figure 3.1 A typical periodic structure on a microstrip substrate 24

Figure 3.2 The sampling path for 2-Level approach (a) on the complex k_ρ plane and (b) on the complex k_{z0} plane 25

Figure 3.3 Comparison of complex image representation of reflection coefficients obtained by 2-level DCIM to the exact values along the sampling path 28

Figure 3.4 Comparison of the approximate (2-Level DCIM) and exact periodic Green's functions at observation point $\rho = 0.78\lambda_0$ 28

Figure 3.5 Relative error between the approximate (2-Level DCIM) and the exact periodic Green's functions at observation point $\rho = 0.78\lambda_0$ 29

Figure 3.6 Comparison of approximate (2-Level DCIM) and exact spectral domain Green's functions along the real axis of the $k_\rho - plane$ 29

Figure 3.7 Comparison of approximate (2-Level DCIM with surface wave extraction) and exact spectral domain Green's functions along the real axis of the $k_\rho - plane$. 32

Figure 3.8 Relative error between the approximate (2-Level DCIM with surface wave extraction) and exact spectral domain Green's functions along the real axis of the $k_\rho - plane$ 32

Figure 3.9 Comparison of the approximate (2-Level DCIM with surface wave extraction) and exact periodic Green's functions at observation point $\rho = 0.78\lambda_0$ 33

Figure 3.10 Relative error between the approximate (2-Level DCIM with surface wave extraction) and the exact periodic Green's functions at observation point $\rho = 0.78\lambda_0$ 33

Figure 3.11 The sampling path for 3-Level approach (a) on the complex k_ρ plane and (b) on the complex k_{z0} plane 34

Figure 3.12 Relative error between the approximate (3-Level DCIM with surface wave extraction) and exact spectral domain Green's functions along the real axis of the $k_\rho - plane$ 36

Figure 3.13 Comparison of the approximate (3-Level DCIM with surface wave extraction) and exact periodic Green's functions at observation point $\rho = 0.78\lambda_0$ 37

Figure 3.14 Relative error between the approximate (3-Level DCIM with surface wave extraction) and the exact periodic Green's functions at observation point $\rho = 0.78\lambda_0$ 37

Figure 3.15 Magnitudes of the approximate (3-Level DCIM with surface wave extraction) and exact periodic Green's functions at observation points along the diagonal of a unit cell 38

Figure 3.16 Relative error between the approximate (3-Level DCIM with surface wave extraction) and exact periodic Green's functions at observation points along the diagonal of a unit cell 38

Figure 4.1 Convergence of the spectral summation for the surface wave contribution . 43

Figure 4.2 Convergence of the spectral series of Ewald summation for $E = 0.7E_{opt}$ . . 44

Figure 4.3 Convergence of the spatial series of Ewald summation for $E = 0.7E_{opt}$ . . 44

Figure 4.4 Convergence of the spectral series of Ewald summation for $E = E_{opt}$ . . . 45

Figure 4.5 Convergence of the spatial series of Ewald summation for $E = E_{opt}$ 45

Figure 4.6 Convergence of the spectral series of Ewald summation for $E = 1.6E_{opt}$ . . 46

Figure 4.7 Convergence of the spatial series of Ewald summation for $E = 1.6E_{opt}$ . . 46

Figure 4.8 Convergence of Ewald summation for the reflected term of the Green's function 47

Figure 4.9 Comparison of the approximate Green's function accelerated by Ewald summation with approximate and exact Green's functions with no acceleration . . 48

Figure 4.10 Convergence of the spectral series of Ewald summation for $a = b = 4.3\lambda_0$ and $E = E_{opt}$ 49

Figure 4.11 Convergence of the spatial series of Ewald summation for $a = b = 4.3\lambda_0$ and $E = E_{opt}$ 49

Figure 4.12 Convergence of the spectral series of Ewald summation for $a = b = 4.3\lambda_0$ and $E = 2E_{opt}$ 50

Figure 4.13 Convergence of the spatial series of Ewald summation for $a = b = 4.3\lambda_0$ and $E = 2E_{opt}$ 50

CHAPTER 1

INTRODUCTION

A periodic structure in a multilayered media can be formed either by periodically implanting dielectric gratings into a layer (Figure 1.1) or by periodically loading a layer with conducting patches and/or vias (Figure 1.2). These kind of periodic structures can be employed as Frequency Selective Surfaces (FSS), reflect arrays, metamaterials or Electromagnetic Bandgap Structures (EBG) which have been widely used in electromagnetic applications. The application areas of these structures cover efficient, low profile antennas [1], directive resonator antennas [2], high Q filters and resonators [3], Radar Absorbing Materials (RAM) [4], left-handed materials [5], etc.

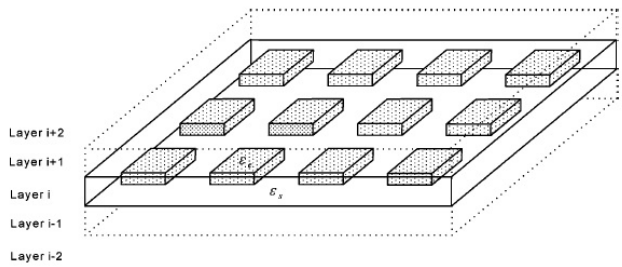

Figure 1.1: Periodic structure with dielectric gratings [8]

The capabilities of these kind of structures attracted many researchers and the rigorous analysis of them gained importance. FEM [6] and Method of Moments (MoM) [7] are generally used in the numerical analysis of periodic structures. FEM is applied as an hybrid technique in conjunction with an integral equation method. In this approach, the structure is considered to be a combination of an inhomogeneous region and a homogeneous region. The inhomogeneous region is the part which includes the implanted material blocks. FEM is used in this

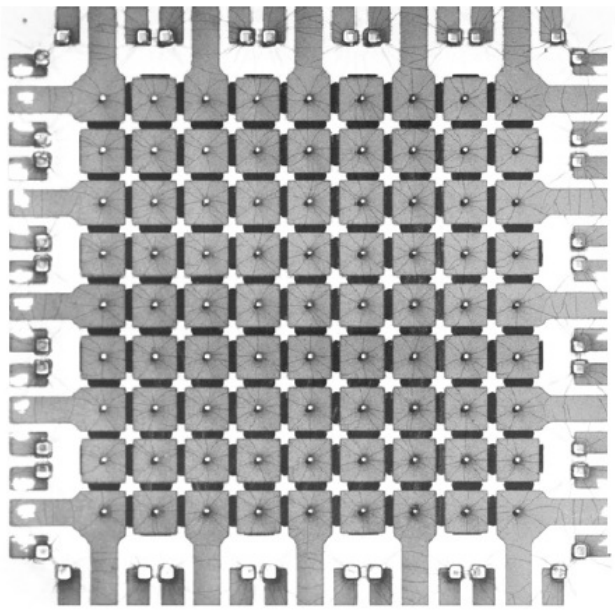

Figure 1.2: Example of a periodic structure with conducting patches (a 2-D mushroom type left-handed material) [5]

part because of its effectiveness in handling the inhomogeneities. The homogeneous region is the part above and below the material blocks. Integral equation methods such as MoM or Boundary Integral (BI) method are applied in this homogeneous region since they are very efficient in modeling open radiating structures. Because of its more straightforward application compared to hybrid approach, MoM is the preferred technique in this work.

MoM analysis of periodic structures in layered media results in a matrix equation (ZI=V) in terms of the surface current densities induced on the conductors and equivalent volume current densities that model the dielectric gratings. The construction of the Z matrix requires the evaluation of the periodic Green's function in layered media. The periodic Green's function can be expressed as an infinite series over the Floquet modes of the spectral domain Green's function:

$$G = \frac{1}{ab} \sum_{m=-\infty}^{\infty} \sum_{n=-\infty}^{\infty} \tilde{G}_{mn}(k_{xm}, k_{yn}) e^{-jk_{xm}(x-x')} e^{-jk_{yn}(y-y')} \tag{1.1}$$

$$k_{xm} = k_x^i + \frac{2\pi m}{a} \tag{1.2}$$

$$k_{yn} = k_y^i + \frac{2\pi n}{b} \tag{1.3}$$

$$k_x^i = k_0 \sin\theta \cos\phi \tag{1.4}$$

$$k_y^i = k_0 \sin\theta \sin\phi \tag{1.5}$$

where G is the spatial domain periodic Green's function, $\tilde{G}_{mn}$ is the spectral domain Green's function of a single element, a and b are the periodicities in x and y directions, respectively, while θ and ϕ are the polar and azimuthal angles of an incident or scattered wave.

Consequently, the CPU time required for the calculation of the periodic Green's function constitutes a large percentage of the total solution time. Moreover, if the MoM analysis of the structure has to be repeated for a large number of frequency points (to obtain the frequency response of the structure), some acceleration techniques need to be developed to reduce the computation time.

The utilization of Pade approximation in the MoM analysis of periodic structures is proposed in [8] to eliminate the need for the repeated calculations of the current vector, I, at each frequency point. In this method, the current vector is approximated by a rational function of two polynomials as:

$$I(f) \approx \frac{a_0 + a_1(f - f_a) + ... + a_p(f - f_a)^p}{1 + b_1(f - f_a) + ... + b_q(f - f_a)^q} \tag{1.6}$$

The coefficients $a_0, ..., a_p; b_1, ..., b_q$ in the polynomials are calculated by equating the Pade approximation given in equation 1.6 to the Taylor series expansion of the current up to the order $p + q$. The coefficients in the Taylor series expansion correspond to the moments of the current and their evaluation requires the computation of the high order derivatives of the Z matrix at the expansion frequency.

However, the computation of the high order derivatives of the periodic Green's function, and thus the Z matrix, is difficult and time consuming because of the complexity of the Green's function expressions in layered media. This complexity is due to the iterative relations involved in the generalized Fresnel reflection coefficients that appear in the spectral domain Green's function expressions of the layered media. This complexity might be reduced by approximating the reflection coefficients in terms of complex exponentials through the use of Discrete Complex Image Method (DCIM) [21], [23], [24], [27]. Once the DCIM approximation is obtained at the expansion frequency, the higher order derivatives of the Green's

function can be easily obtained by assuming that the exponents and the coefficients found via DCIM are not significantly dependent on frequency. This assumption is verified in [9] where Pade approximation is used in conjunction with the DCIM in the MoM analysis of printed structures. The numerical results presented in [9] for the analysis of a coupled line filter show that the exponents and the coefficient found via DCIM at a single frequency can be assumed to be constant over a 10% bandwidth. Therefore, the main motivation of this thesis is to apply the DCIM in the evaluation of the periodic Green's function for the layered media in order to efficiently compute the high order derivatives of the Green's function required for the application of the Pade approximation method.

The utilization of DCIM for the efficient numerical evaluation of the Green's function for periodic structures in layered media was proposed by various researchers [10], [11], [12]. In these works, the spectral domain Green's function is decomposed into two parts: i) the asymptotic component that corresponds to the complex exponential approximation and ii) the remainder part that is left after the subtraction of the asymptotic part from the exact Green's function. As it will be presented in Chapter 2, the DCIM makes it possible to cast the Green's function in layered media into a form similar to the free space Green's function. It is demonstrated that computation of the periodic free space Green's function can be accelerated through the use of the Ewald transformation [32], [33]. Therefore, a similar acceleration for the numerical evaluation of the periodic Green's function in layered media can be achieved when the DCIM is utilized. [11] and [12] exploit this fact and accelerate the asymptotic series summation by using Ewald's Method. After the extraction of the asymptotic part, the remainder part becomes rapidly convergent compared to the original Green's function. In [12], the summation for this remainder part is computed by using Shanks' Transformation [14], [15].

Although the periodic Green's function in layered media was accurately and efficiently computed in these works, they do not offer any simplification for the computation of the derivatives of the Green's function with respect to frequency since the original Green's function expression still exists in the remainder part of the Green's function. Therefore, the remainder part needs to be eliminated for the efficient computation of the derivatives with respect to frequency. Although the complex exponential approximation is obtained by sampling the spectral domain Green's function, the remainder term is non-zero. This is due to the fact that some part of sampling needs to be done over the complex values of spectral variable k_ρ in order not to cross the surface wave poles, but the Floquet mode summation is over real values

of k_ρ. Therefore, the sampling should also be done along the real k_ρ axis in order to eliminate the remainder term. For this aim, the 3-level DCIM proposed in [27] is used to approximate the spectral domain Green's functions. It should be noted that in order to be able to perform the sampling over the real values of k_ρ, the surface wave contributions need to be extracted prior to sampling.

In the second chapter of this thesis, some background information about the Discrete Complex Image Method, the surface wave pole extraction procedure and Ewald's Method are presented. Various forms of DCIM like 2-Level and 3-Level schemes are introduced. A brief introduction for series acceleration techniques is given and then the Ewald's transformation is summarized.

Chapter 3 presents the numerical results obtained by approximating the Green's function for periodic structures in planarly layered media with complex exponentials through the application of DCIM. In order to demonstrate the accuracy achieved with the use of 3-Level DCIM, the numerical results obtained by 2-Level DCIM with and without surface wave extraction are also included.

Chapter 4 is reserved for the acceleration of the computation of the periodic Green's function in layered media by using Ewald's transformation. First, the modifications made in Ewald's transformation associated with the complex exponentials are introduced, then the numerical results are presented.

The final chapter is devoted for the conclusions of this thesis work including the advantages and shortcomings of the proposed method. Future work that is planned to be accomplished is also discussed.

The software used throughout this thesis work is MATLAB.

CHAPTER 2

BACKGROUND INFORMATION

2.1 Discrete Complex Image Method

As the printed geometries in multilayer environment have found increasingly more use in the designs of low-profile, light-weight and multifunction antennas, and microwave integrated circuits, rigorous analysis of these structures have become more important. The numerical algorithms based on Method of Moments (MoM) are widely favoured over other techniques to analyze these geometries.

In order to be able to apply the MoM, the expressions for the Green's functions in the corresponding domain are required. However, closed-form Green's functions for planarly layered media can be obtained analytically only in the spectral domain. Closed-form Green's functions in spatial domain are obtained through either a 2-D inverse Fourier transformation or a 1-D Hankel transformation of the corresponding spectral domain function [17]. The latter transformation is also known as the Sommerfeld integral which is expressed as [17]

$$G = \frac{1}{4\pi} \int_{SIP} dk_\rho k_\rho H_0^{(2)}(k_\rho \rho) \tilde{G}(k_\rho) \tag{2.1}$$

where G is the spatial domain Green's function, $\tilde{G}$ is the spectral domain Green's function, $H_0^{(2)}$ is the zeroth order Hankel function of the second kind and SIP is the Sommerfeld Integration Path as shown in Figure 2.1 for a lossless structure. Since both approaches mentioned above involve the evaluation of oscillatory and slowly-convergent integrals some approximation methods need to be applied to compute the spatial domain Green's functions efficiently and accurately.

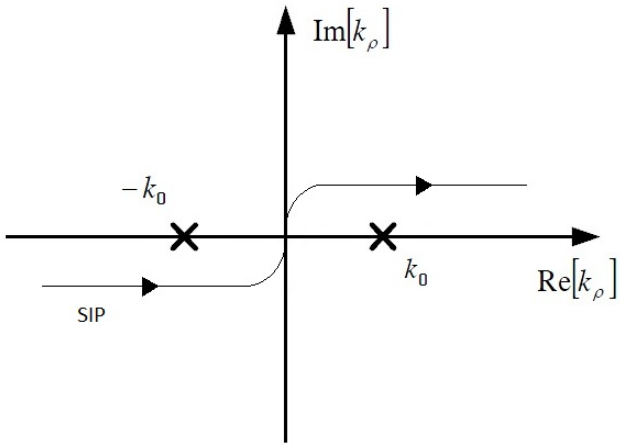

Figure 2.1: Sommerfeld Integration Path

It is first proposed in [23] to approximate the spectral domain Green's functions by complex exponentials so that the Sommerfeld integral can be evaluated analytically by using the well known Sommerfeld identity

$$\frac{e^{-jkr}}{r} = -\frac{j}{2}\int_{SIP} dk_\rho k_\rho H_0^{(2)}(k_\rho\rho)\frac{e^{-jk_z|z|}}{k_z} \tag{2.2}$$

The complex exponential approximation of the spectral domain Green's function can be written in the following form:

$$\tilde{G}(k_\rho) = \sum_{i=1}^{M} \alpha_i \frac{e^{-jk_z\beta_i}}{j2k_z} \tag{2.3}$$

Consequently, by using the Sommerfeld identity, the spatial domain Green's function takes the following form:

$$G(x-x', y-y') = \frac{1}{4\pi}\sum_{i=1}^{M} \alpha_i \frac{e^{-jkR_i}}{R_i} \tag{2.4}$$

where $R_i = \sqrt{(x-x')^2 + (y-y')^2 + \beta_i^2}$. Since this method provides a closed-form expression for the spatial domain Green's function as shown in equation 2.4, initially the method is shortly named as 'closed-form Green's function'. However, later on, researchers working in this area preferred to call the method as 'Discrete Complex Image Method (DCIM)', since

each term of the summation in equation 2.4 represents the contribution of a complex source with amplitude α_i positioned at a complex distance β_i.

The originally proposed DCIM, is further studied in [21] where the total Green's function is decomposed into three components. The first component represents the contribution of the quasi-dynamic images dominating in the near-field region, the second component represents the contribution of the surface waves dominating in the far-field region and finally the third component represents the contribution of the complex images. The spectral domain expressions for the contributions of the quasi-dynamic images and the surface waves are subtracted from the spectral domain Green's function and the remaining part is approximated by DCIM. In order to find the complex coefficients and exponents given in equation 2.3, the remaining part of the spectral domain Green's function is sampled along the path C_1 shown in Figure 2.2. Then the Prony's Method [18] is employed to extract the complex exponent and coefficient information from the sampled data. Prony's method requires the sampling to be performed along a real variable. Therefore, the following transformation is carried out to map the complex variable k_{z0} into a real variable t

$$C_1 : \quad k_{z0} = k_0[-jt + (1 - \frac{t}{T_0})] \quad , 0 \leq t \leq T_0 \tag{2.5}$$

where t is the running parameter and T_0 is the truncation point.

Although the DCIM is more efficient than numerical integration, this method has some problems which are investigated in [24]. Green's functions may have sharp peaks and fast changes for small values of t. This means that, the sampling rate should be high for small values of t so that the fine features of the function is captured in the approximation. T_0 is another parameter of the approximation that effects accuracy and the speed of the algorithm. If a Green's function has a slow-decaying spectral domain behaviour, then one must sample it far enough to get an accurate near-field distribution that means a larger T_0. When the Green's function has sharp peaks and fast changes as well as a slow-decaying spectral domain behaviour, one must sample it to a large T_0 with very small Δt steps in order to get accurate near-field and far-field distribution which causes a long CPU time. If the Green's function does not possess one of the aforementioned properties, we can choose a smaller T_0 or a larger Δt step to make the computations faster. As an example, if the Green's function has a fast-decaying spectral domain behaviour we can choose a smaller T_0 and still obtain an accurate near-field distribu-

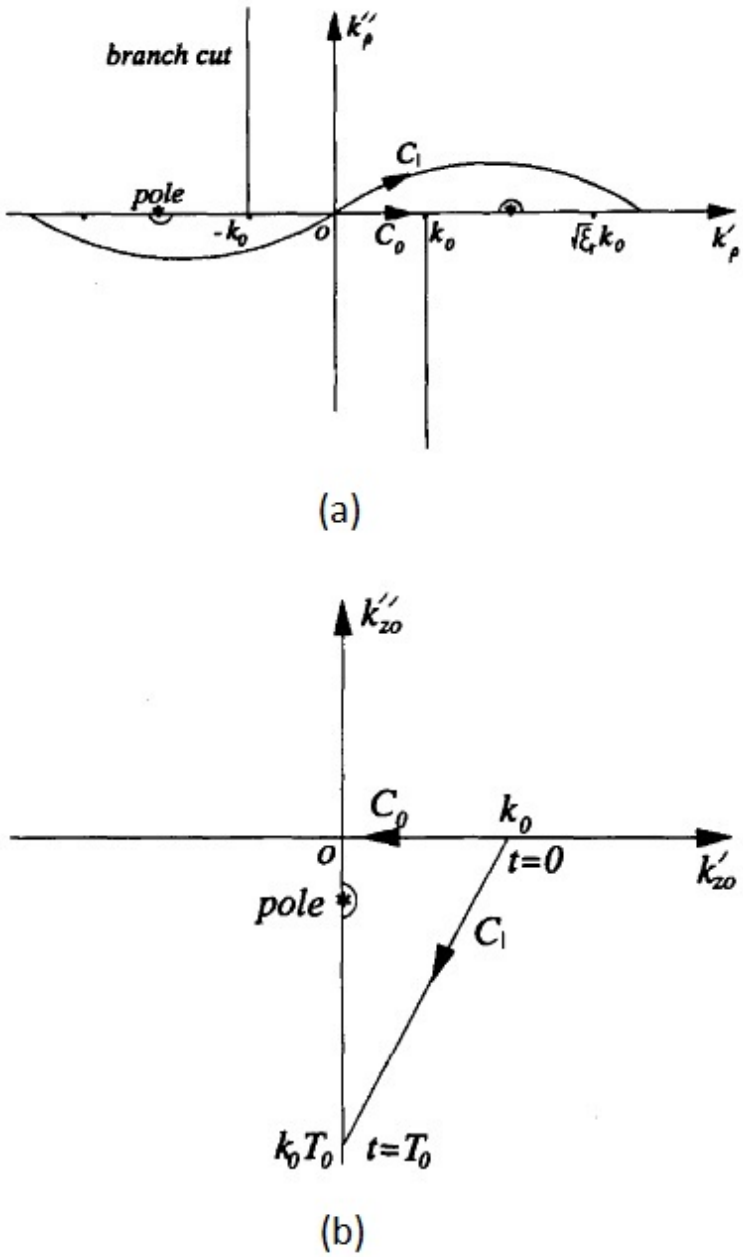

Figure 2.2: The sampling paths on the complex: (a) k_ρ plane and (b) k_{z0} plane [21]

tion with a shorter CPU time. However this requires users to investigate the spectral domain behaviour of the Green's functions in advance and then to perform a few iterations to find the best possible combination of the approximation parameters. Because of these difficulties, the one-level approximation approach as studied in [21] can not be made fully robust and suitable for the development of computer aided design tools. M. I. Aksun developed a two-level approach [24] in order to overcome these problems. There are two paths instead of one as

seen in Figure 2.3. The first path is a simple line on the real axis of k_ρ plane between $k_{\rho_{max2}}$ and $k_{\rho_{max1}}$. The second path is same as the path described in the one-level approach. The Green's function is first sampled along the path C_{ap1} and approximated by complex exponentials. Then, the approximated function is subtracted from the original Green's function and the remaining function is sampled along the path C_{ap2} and it is approximated by another set of complex exponentials. These two sets are then added together to obtain the total closed-form Green's function.

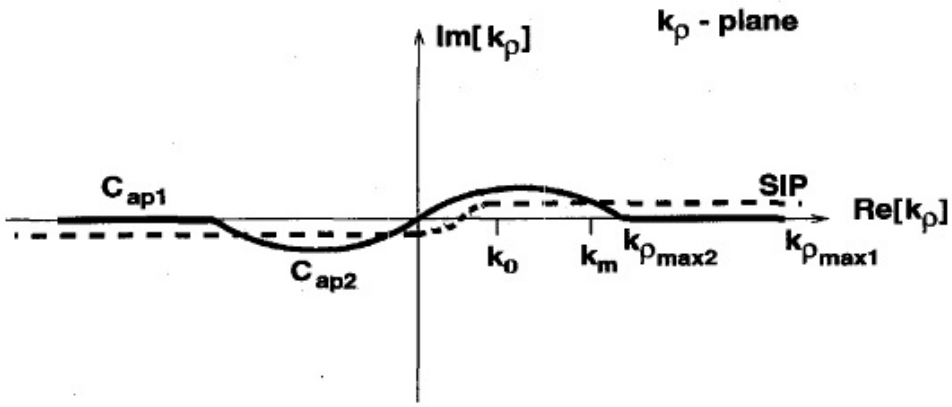

Figure 2.3: The sampling path on the complex k_ρ plane in [24]

Since the sharp peaks and fast changes occur for small k_ρ values, sampling along the path C_{ap1} can be done with large steps and this lets us to make the sampling in a wider range (larger $k_{\rho_{max1}}$) leading to a very accurate near-field distribution. For small k_ρ values, the sampling is performed along the path C_{ap2} with small steps to capture the fine features (fast changes, peaks), but this time a narrower sampling interval (smaller $k_{\rho_{max2}}$) could be chosen so that the total number of sampling points and consequently the CPU time for the computation stays at low values compared to one-level approximation. This method also has the advantage of being versatile since it is applicable to all kinds of Green's functions without changing the approximation parameters. It should also be noted that for the extraction of complex coefficients and exponents, Generalized Pencil of Function (GPOF) method [19] is preferred rather than Prony's method in the two-level approximation scheme since GPOF method is less sensitive to numerical noise.

Although being successful in approximating the Green's function for distances up to a few wavelengths ($\rho = 3\lambda, 4\lambda$), the accuracy of the method deteriorates beyond this range. In

the literature, the reason of this problem is attributed mainly to two sources; not extracting the quasi-static terms and not extracting the surface wave contributions before applying the DCIM.

However, as discussed in [25], in the application of the two-level approach, the approximation of the spectral domain Green's functions on the path C_{ap1} via complex exponentials can be considered as the extraction of the quasi-static terms in addition to some dynamic terms. Moreover, it is demonstrated in [25] through numerical examples that the difference between the approximation of the surface wave contribution by complex exponentials and the exact surface wave contribution is responsible for the deviation of the complex image approximation of the Green's function from the exact Green's function beyond a few wavelengths. The reason of this result is attributed to the fact that the terms approximated by complex images represent spherical waves while the original surface wave contributions are cylindirical in nature. Hence, if the dimensions of the structure under investigation is larger than a few wavelengths, surface wave contributions must be subtracted from the spectral domain Green's function prior to the complex image approximation and their contributions must be added analytically in the spatial domain to obtain more accurate results. As pointed out in [26], there is still an important shortcoming of the two-level approximation scheme resulting from its lack of capturing the contribution of the lateral waves associated with the branch point singularity.

The surface waves have the following asymptotic behaviour for large ρ [27]:

$$\frac{e^{-jk_{\rho p}\rho}}{\sqrt{\rho}} \tag{2.6}$$

where $k_{\rho p}$ is the surface wave pole (SWP), whereas lateral waves at an interface of two materials behave asymptotically like [28]:

$$\frac{e^{-jk_{br}\rho}}{\rho^2} \tag{2.7}$$

where k_{br} is the branch point, which is usually a real quantity. A simple comparison of equations 2.6 and 2.7 reveals that when a SWP ($k_{\rho p}$) is purely real (lossless material), the contribution of the surface waves dominate in the far field and the two-level approach with SWP extraction does not fail in the far field regions. On the other hand, if a SWP has an

imaginary part (it must be negative imaginary), as in the cases of lossy materials, its contribution decays exponentially with increasing ρ whereas the contribution of the lateral waves decay with ρ^2. Therefore, for such cases, the contribution from the lateral waves determine the far-field behaviour of the spatial domain Green's functions and the two-level approach fails in the far field regions even though the surface wave contributions are extracted.

As proposed in [27], in order to incorporate the contribution of the lateral waves, the sampling path of the two-level approach needs to be modified such that the DCIM become capable of capturing the features around the branch point accurately. To achieve this goal, three different sampling paths are suggested which are shown in Figures 2.4, 2.5 and 2.6. All of the three approaches presented, are designed to bring the sampling paths closer to the branch point k_0.

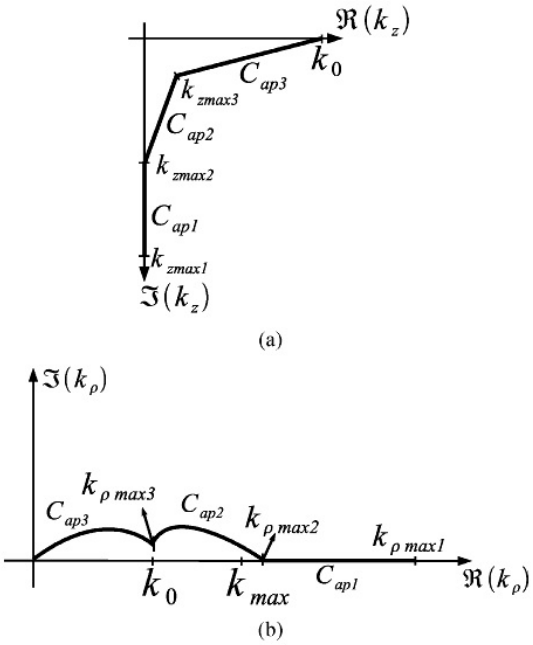

Figure 2.4: Path for the first 3-level DCIM approach on the complex: (a) k_z plane and (b) k_ρ plane [27]

It can be observed that the sampling should be done over three different paths in order to be able to take samples close to the branch point k_0. Hence this method is referred as 'Three-level approximation scheme'.

The formulation presented so far is valid for a single hertzian dipole source. When a periodic source configuration is considered, the spatial domain Green's functions could be obtained from their spectral domain counterparts through the use of the following Floquet mode sum-

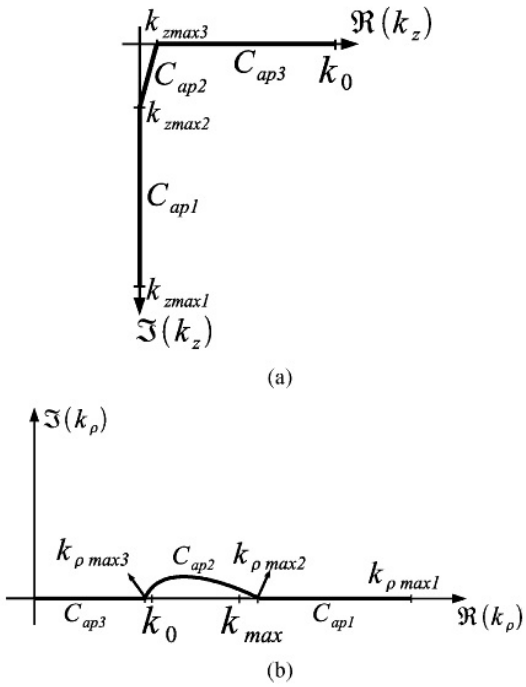

Figure 2.5: Path for the second 3-level DCIM approach on the complex: (a) k_z plane and (b) k_ρ plane [27]

mations:

$$G = \frac{1}{ab} \sum_{m=-\infty}^{\infty} \sum_{n=-\infty}^{\infty} \tilde{G}_{mn}(k_{xm}, k_{yn}) e^{-jk_{xm}(x-x')} e^{-jk_{yn}(y-y')} \tag{2.8}$$

For a single source, the sampling path in the DCIM can be freely modified to improve the accuracy of the method as long as the deformed path does not cross any singularities. Because the relation between the spectral and the spatial domain Green's functions are in terms of Fourier integrals, the modifications on the integration path does not affect the result of the integral according to the Cauchy integral theorem. However, for the case of periodic sources, one does not have the freedom to choose the sampling path of the DCIM. Since the Floquet mode summation is over the real values of k_x and k_y, and hence k_ρ, the sampling of the spectral domain Green's function should also be performed along the real values of k_ρ. Hence the three-level approximation scheme is employed in this thesis with a sampling path along the real k_ρ axis. It is apparent that for this choice of sampling path, the surface wave contributions need to be extracted before applying DCIM. Therefore, the surface wave extraction procedure will be outlined in the next section.

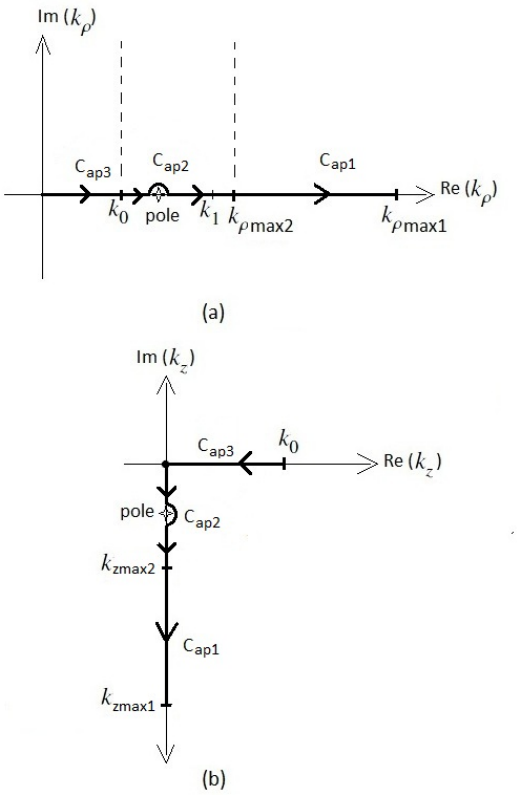

Figure 2.6: Path for the third 3-level DCIM approach on the complex: (a) k_ρ plane and (b) k_z plane [27]

2.2 Surface Wave Poles

The Green's functions for the cases of layered media involve poles and branch point singularities. These singularities are responsible for the surface and lateral waves excited by the source. The surface waves are of high importance since they can propagate along the interface without suffering much attenuation [29].

Surface wave poles always exist in pairs, negative of each other, on the complex k_ρ plane [27]. Therefore, the surface wave contribution of a pole pair can be represented in the spectral domain as

$$\tilde{G}_{sw} = \frac{2k_{\rho p}Res}{k_\rho^2 - k_{\rho p}^2} \tag{2.9}$$

where $k_{\rho p}$ is the surface wave pole and Res is the residue of it. Surface wave poles and the associated residues for a general multilayer media can be obtained via the method presented

in [31], which is easy and robust. By using the residue theorem, the contribution of these poles in the spatial domain can be easily expressed as:

$$G_{sw} = -\frac{j}{2}(Res)H_0^{(2)}(k_{\rho p}\rho)k_{\rho p} \tag{2.10}$$

It is known [30] that for large arguments, the Hankel function of the second kind decays with the square-root of the argument. Since the spherical waves decays with ρ itself, in far fields the surface waves become dominant over spherical waves, which is the reason why surface wave poles must be extracted and handled explicitly to obtain an accurate far field distribution.

The spatial domain Green's function for the case of periodic sources is obtained via Floquet mode summations. This summation is applied for both the complex exponentials obtained by DCIM and the spectral domain surface wave contribution which is given in equation 2.9. Thus, the periodic Green's function in spatial domain is expressed as follows:

$$G = \frac{1}{ab}\sum_{m=-\infty}^{\infty}\sum_{n=-\infty}^{\infty}\sum_{i=1}^{M}\alpha_i\frac{e^{-jk_{z0}\beta_i}}{j2k_{z0}}e^{-jk_{xm}(x-x')}e^{-jk_{yn}(y-y')}+\frac{1}{ab}\sum_{m=-\infty}^{\infty}\sum_{n=-\infty}^{\infty}\frac{2k_{\rho p}Res}{k_\rho^2-k_{\rho p}^2}e^{-jk_{xm}(x-x')}e^{-jk_{yn}(y-y')} \tag{2.11}$$

where x' and y' are the coordinates of the source; x and y are the coordinates of the observation point; a and b are the periodicities of the structure in x and y directions, respectively; k_{xm} and k_{yn} are the wavenumbers in x and y directions, respectively and k_{z0} is the wavenumber in z direction. Note also that, α_i and β_i are the coefficients and exponents obtained by applying DCIM to the spectral domain Green's function in layered media. k_{xm}, k_{yn} and k_{z0} are given as

$$k_{xm} = k_x^i + \frac{2\pi m}{a} \tag{2.12}$$

$$k_{yn} = k_y^i + \frac{2\pi n}{b} \tag{2.13}$$

$$k_{z0} = \begin{cases} \sqrt{k_0^2 - (k_{xm}^2 + k_{yn}^2)} & k_0^2 \geq k_{xm}^2 + k_{yn}^2 \\ -j\sqrt{(k_{xm}^2 + k_{yn}^2) - k_0^2} & k_0^2 \leq k_{xm}^2 + k_{yn}^2 \end{cases} \tag{2.14}$$

where k_x^i and k_y^i are the wavenumbers associated with $m = 0$ and $n = 0$ respectively. They are given as

$$k_x^i = k_0 \sin\theta \cos\phi \tag{2.15}$$

$$k_y^i = k_0 \sin\theta \sin\phi \tag{2.16}$$

where θ and ϕ are the polar and azimuthal angles of an incident or scattered wave.

The expression in equation 2.11 is a spectral summation. The spatial domain periodic Green's function can also be expressed as a spatial summation by applying Poisson transformation to equation 2.11. The two-dimensional Poisson's summation formula is given in [10] as follows:

$$\sum_{m=-\infty}^{\infty}\sum_{n=-\infty}^{\infty} f(ma, nb) = \frac{1}{ab}\sum_{m=-\infty}^{\infty}\sum_{n=-\infty}^{\infty} F(\frac{2\pi m}{a}, \frac{2\pi n}{b}) \tag{2.17}$$

where $f(x, y)$ and $\mathrm{F}(k_x, k_y)$ are a Fourier transform pair in two dimensions. Their relation are given by the equations below:

$$F(k_x, k_y) = \int_{-\infty}^{\infty}\int_{-\infty}^{\infty} f(x, y) e^{-j(k_x x + k_y y)} dxdy \tag{2.18}$$

$$f(x, y) = \frac{1}{4\pi^2}\int_{-\infty}^{\infty}\int_{-\infty}^{\infty} F(k_x, k_y) e^{+j(k_x x + k_y y)} dk_x dk_y \tag{2.19}$$

The spatial summation expression for the periodic Green's function is then obtained as:

$$G = \sum_{m=-\infty}^{\infty}\sum_{n=-\infty}^{\infty}\sum_{i=1}^{M} \alpha_i \frac{e^{-jk_0 R_i}}{4\pi R_i} e^{-jk_x^i ma} e^{-jk_y^i nb} + \sum_{m=-\infty}^{\infty}\sum_{n=-\infty}^{\infty} -\frac{j}{2}(Res) H_0^{(2)}(k_{\rho p}\rho) k_{\rho p} e^{-jk_x^i ma} e^{-jk_y^i nb} \tag{2.20}$$

where $R_i = \sqrt{(x - x' - ma)^2 + (y - y' - nb)^2 + \beta_i^2}$. The first part of the right-hand side of equation 2.20 is the summation of complex exponentials in spatial domain and the second one is the summation of spatial domain surface wave contributions. The exponential term in equation 2.20 is in the same form as free space Green's function except that there is a complex coefficient in front of it and the expression for the distance between the source and observation point is different here. Because of this similarity, Ewald's transformation, which is succesfully utilized to accelerate the summation of the free space periodic Green's function, can also be applied to equation 2.20. Therefore, Ewald's transformation will be presented in the next section.

2.3 Ewald's Transformation

The main idea behind the series acceleration techniques is to transform a slowly convergent sequence into a faster converging sequence by using a mapping. There is neither a universal algorithm that works for every type of sequence nor a unique algorithm that works for a type of sequence. One can also use a combination of several algorithms in a problem.

Kummer's transformation [16] is a widely used technique in series acceleration. It makes use of the fact that the rate of convergence of a series is determined by the asymptotic form of that series. If $f(m,n)$ is asymptotic to a function $f_1(m,n)$ which is defined for all integers n, then Kummer's transformation yields [13]

$$\sum_{m=-\infty}^{\infty}\sum_{n=-\infty}^{\infty} f(m,n) = \sum_{m=-\infty}^{\infty}\sum_{n=-\infty}^{\infty} [f(m,n) - f_1(m,n)] + \sum_{m=-\infty}^{\infty}\sum_{n=-\infty}^{\infty} f_1(m,n) \tag{2.21}$$

Generally, $f_1(m,n)$ is chosen in such a way that the last series in equation 2.21 has a known closed-form expression. If a known closed-form expression is not available, then one can use a transformation to make it rapidly convergent. This is the case in [13] where the spectral domain expression of free space Green's function for doubly periodic structures is first divided into two parts by Kummer's Transformation. The first part becomes rapidly convergent since the asymptotic expression is subtracted. The other part, which is asymptotic and slowly convergent is recognized as the spectral representation of the original periodic source distribution radiating in a medium with an imaginary wavenumber. Then, Poisson transformation is applied to change it into a spatial domain expression. In this way, the slowly convergent series at the beginning, has been transformed into two rapidly convergent series.

It is the reciprocal spreading property of the Fourier transformation that makes Poisson transformation so beneficial for the acceleration of the series. If a function is smooth and approaches zero gradually as its argument goes to infinity, then its Fourier transform is highly localized and the corresponding sum converges rapidly.

For the cases of periodic structures in layered media, things are more complex than the free space case because of the reflection coefficient in the spectral domain Green's function expressions. In [12], Shanks transformation is applied directly to the periodic Green's functions in planarly stratified structures and it is shown that straightforward Shank transformation can

efficiently calculate the periodic Green's function. However, it is reported in that work that the efficiency of Shanks transformation is severely reduced when the distance between the observation and the source points approaches zero or one period. Therefore, we need a better method in order to accelerate the summation in such cases. Ewald transformation is a good solution because of its Gaussian decaying characteristics.

In 1921, P. P. Ewald, who was studying on the calculation of Coulomb interaction energy for a lattice of ions, published a work [32] in which he presented a method for speeding up the convergence of series appearing in certain lattice sums. Its computational results was so successful that researchers from various fields have adapted and applied the technique to their own problems. Three of these researchers have applied Ewald's method to the problem of efficient numerical evaluation of the free space Green's function for periodic structures [33]. The method is also adapted to the cases of two-dimensional problems with one-dimensional periodicity [34] and three-dimensional problems with one-dimensional periodicity [35]. Its application in evaluating Green's functions for multilayered media is treated in [36], [11], [12] and its application in evaluating Green's functions for a rectangular cavity is handled in [37].

Here, the application of Ewald method to the free space periodic Green's function (FSPGF) will be summarized. Modifying it for the case of planarly layered media is a simple task and it will be performed in Chapter 4.

FSPGF can be expressed in terms of a spectral sum as follows:

$$\tilde{G} = \frac{1}{ab} \sum_{m=-\infty}^{\infty} \sum_{n=-\infty}^{\infty} \frac{e^{-jk_{z0}(z-z')}}{j2k_{z0}} e^{-jk_{xm}(x-x')} e^{-jk_{yn}(y-y')} \tag{2.22}$$

By using the Poisson transformation, it can also be expressed in terms of a spatial sum as

$$G = \frac{1}{4\pi} \sum_{m=-\infty}^{\infty} \sum_{n=-\infty}^{\infty} \frac{e^{-jk_0 R}}{R} e^{-jk_x^i ma} e^{-jk_y^i nb} \tag{2.23}$$

where R is the distance between the observation point at (x, y, z) and the $(m, n)^{th}$ periodic source point located at $(x' + ma, y' + nb, z')$. The expression for R is

$$R = \sqrt{(x - x' - ma)^2 + (y - y' - nb)^2 + (z - z')^2} \tag{2.24}$$

The method of Ewald is based on the following formula [32]:

$$\frac{e^{-jkR}}{R} = \frac{2}{\sqrt{\pi}} \int_0^{\infty} e^{-R^2 s^2 + \frac{k^2}{4s^2}} ds \tag{2.25}$$

Here, s is a complex variable. For the validity of this equation, the path of integration must be chosen such that the integrand remains bounded as $s \to 0$ and decays as $s \to \infty$. This means that

$$arg(s) \in \begin{cases} [\alpha_k - 3\pi/4, \alpha_k - \pi/4] & s \to \infty \\ [-\pi/4, \pi/4] & s \to 0 \end{cases} \tag{2.26}$$

During the application of the Ewald method, a change of variable from s to s' ($s' = 1/s$) is required [33]. When this is done, the integrand must still remain bounded as $s' \to 0$ and decays as $s' \to \infty$. This is possible if one chooses an integration path which lies in the intersection of the two regions defined in equation 2.26. In other words, as $s \to 0$ and $s \to \infty$,

$$arg(s) \in \begin{cases} [-\pi/4, \alpha_k - \pi/4] & \alpha_k \in [0, \pi/2] \\ [\alpha_k - 3\pi/4, \pi/4] & \alpha_k \in [\pi/2, \pi] \end{cases} \tag{2.27}$$

Having defined the necessary integration path (see Figure 2.7), we now use equation 2.25 in expression 2.23 and split the path of integration at E to write the Green's function in two parts as shown below:

$$G = G_1 + G_2 \tag{2.28}$$

$$G_1 = \frac{1}{4\pi} \sum_{m=-\infty}^{\infty} \sum_{n=-\infty}^{\infty} e^{-jk_x^i ma} e^{-jk_y^i nb} \frac{2}{\sqrt{\pi}} \int_0^{E} e^{-R^2 s^2 + \frac{k_0^2}{4s^2}} ds \tag{2.29}$$

$$G_2 = \frac{1}{4\pi} \sum_{m=-\infty}^{\infty} \sum_{n=-\infty}^{\infty} e^{-jk_x^i ma} e^{-jk_y^i nb} \frac{2}{\sqrt{\pi}} \int_E^{\infty} e^{-R^2 s^2 + \frac{k_0^2}{4s^2}} ds \tag{2.30}$$

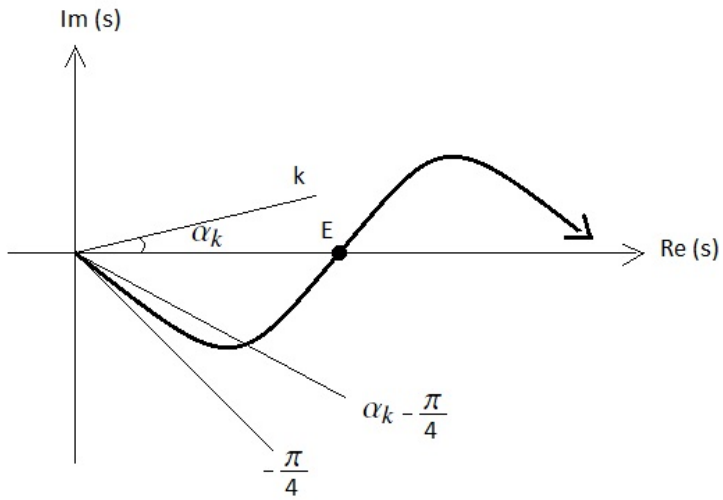

Figure 2.7: Path of integration for the case $\alpha_k \in [0, \pi/2]$

For the second part of the Green's function (equation 2.30) Ewald's formula [32] apply directly, which is shown below:

$$\frac{2}{\sqrt{\pi}} \int_E^{\infty} e^{-R^2 s^2 + \frac{k_0^2}{4s^2}} ds = \frac{1}{2R}[e^{-jk_0 R} erfc(RE - \frac{jk_0}{2E}) + e^{jk_0 R} erfc(RE + \frac{jk_0}{2E})] \tag{2.31}$$

This changes the second part of the Green's function into the expression below:

$$G_2 = \frac{1}{8\pi} \sum_{m=-\infty}^{\infty} \sum_{n=-\infty}^{\infty} \frac{e^{-j(k_x^i ma + k_y^i nb)}}{R} \sum_{\pm} e^{\pm jk_0 R} erfc(RE \pm \frac{jk_0}{2E}) \tag{2.32}$$

We can not apply the Ewald's formula to the first part of the Green's function directly. Instead one can apply it after some mathematical operations [33] and obtain the new expression for G_1 as below:

$$G_1 = \frac{1}{4ab} \sum_{m=-\infty}^{\infty} \sum_{n=-\infty}^{\infty} \frac{e^{-j[k_{xm}(x-x') + k_{yn}(y-y')]}}{jk_{z0}} \sum_{\pm} e^{\pm jk_{z0}(z-z')} erfc(\frac{jk_{z0}}{2E} \pm (z - z')E) \tag{2.33}$$

Now, we have transformed the original slowly converging FSPGF expression, by the Ewald method, into two rapidly decaying expressions. This rapid convergence is because of the $erfc$ function appearing in both series. It is the complementary error function (since its argument

is complex here, it is sometimes referred to as $cerfc$ which means complex complementary error function) and it behaves asymptotically like [33]

$$\frac{e^{-z^2}}{z} \tag{2.34}$$

The only thing left undescribed in the expressions above is the splitting parameter E. When the equations 2.33 and 2.32 are observed, one can see that increasing E has the effect of making the terms in G_1 decay faster while making those in G_2 decay more slowly. If we think in terms of efficiency, the best choice for E is that which balances the rate of decay for both series. By comparing the terms in the two series for large m and n and using the asymptotic expression for $erfc$, it is obtained in [33] that

$$E_{opt} = \sqrt{\frac{\pi}{ab}} \tag{2.35}$$

This E value is optimum in terms of efficiency, but it is shown in [38] that when the periodic spacing becomes large relative to a wavelength, E_{opt} has an accuracy problem. The reason for this problem is explained in [38] as follows. For large arguments, complementary error function behaves as $\frac{e^{-z^2}}{z}$, as stated previously. For large periodic spacings, E_{opt} given in equation 2.35 becomes small and the imaginary part of the argument of $erfc(.)$ becomes large and dominant for the first several terms of the series. As a concequence, $erfc(.)$ becomes very large and therefore one gets very large numbers for the first several terms of these series. Similar comments can be made for both series. Gaussian decay is again achieved for terms with large indices and the two series G_1 and G_2 converge to very large numbers which are nearly equal in magnitude but of opposite sign. Therefore, one suffers severe accuracy loss upon adding the sums of the two series due to finite precision. The result is the convergence to incorrect values. The remedy to this accuracy loss is to increase E beyond E_{opt} in cases of large periodic spacings.

In the next chapter, the numerical results obtained by applying the DCIM to the evaluation of the periodic Green's function in layered media will be presented. The accuracy levels of 2-level and 3-level approximation schemes will be compared.

CHAPTER 3

NUMERICAL RESULTS FOR THE COMPUTATION OF THE PERIODIC GREEN'S FUNCTION IN LAYERED MEDIA

In this chapter, the procedure for the application of the DCIM to the computation of the periodic Green's function in layered media will be outlined and numerical results will be presented. The results obtained through 2-level and 3-level approximation schemes will be compared in order to demonstrate the accuracy improvement achieved with the use of 3-level approximation scheme.

The periodic Green's function (in spatial domain) can be expressed in terms of a spectral sum with the general form as

$$G = \frac{1}{ab} \sum_{m=-\infty}^{\infty} \sum_{n=-\infty}^{\infty} \tilde{G}(k_{xm}, k_{yn}) e^{-jk_{xm}(x-x')} e^{-jk_{yn}(y-y')} \tag{3.1}$$

where k_{xm} and k_{yn} are given as

$$k_{xm} = k_x^i + \frac{2\pi m}{a} \tag{3.2}$$

$$k_{yn} = k_y^i + \frac{2\pi n}{b} \tag{3.3}$$

In equation 3.1, $\tilde{G}$ represents the spectral domain Green's function of an infinitesimal dipole point source at (x', y', z'). The spectral domain Green's functions for planarly layered media can be expressed either in terms of generalized Fresnel reflection coefficients [39] or in terms of equivalent transmission line network parameters [40]. Both of the formulations result in the same expressions.

Numerical results will be presented for the scalar potential of an x-directed Horizontal Electric Dipole (HED) which is positioned above a microstrip substrate of thickness h and relative permittivity ϵ_r (Figure 3.1). The scalar Green's function is chosen as a representative example, the same procedure can be applied for the approximation of the vector potential as well. The spectral domain Green's function expression for such a structure is given by the following form of plane wave summations [21]:

$$\tilde{G_q} = \frac{1}{j2k_{z0}}[e^{-jk_{z0}(z-z')} + (R_{TE} + R_q)e^{-jk_{z0}(z+z')}] \tag{3.4}$$

where R_{TE} and R_q are the coefficients that take into account the reflections from the grounded dielectric substrate and are given by

$$R_{TE} = -\frac{r_{10}^{TE} + e^{-j2k_{z1}h}}{1 + r_{10}^{TE}e^{-j2k_{z1}h}} \tag{3.5}$$

$$R_q = \frac{2k_{z0}^2(1-\epsilon_r)(1-e^{-j4k_{z1}h})}{(k_{z1}+k_{z0})(k_{z1}+\epsilon_r k_{z0})(1+r_{10}^{TE}e^{-j2k_{z1}h})(1-r_{10}^{TM}e^{-j2k_{z1}h})} \tag{3.6}$$

Here, r_{10}^{TE} and r_{10}^{TM} are the Fresnel reflection coefficients for the Transverse Electric and Transverse Magnetic waves at the interface between dielectric and air. They are given by

$$r_{10}^{TE} = \frac{k_{z1} - k_{z0}}{k_{z1} + k_{z0}} \tag{3.7}$$

$$r_{10}^{TM} = \frac{k_{z1} - \epsilon_r k_{z0}}{k_{z1} + \epsilon_r k_{z0}} \tag{3.8}$$

with

$$k_{z0}^2 + k_\rho^2 = k_0^2 \tag{3.9}$$

$$k_{z1}^2 + k_\rho^2 = k_1^2 = \epsilon_r k_0^2 \tag{3.10}$$

$$k_\rho^2 = k_{xm}^2 + k_{yn}^2 \tag{3.11}$$

The spectral domain Green's function expressions for scalar and vector potentials due to a horizontal and/or vertical electric and/or magnetic current source in a multilayer media can be found in [39] or [40].

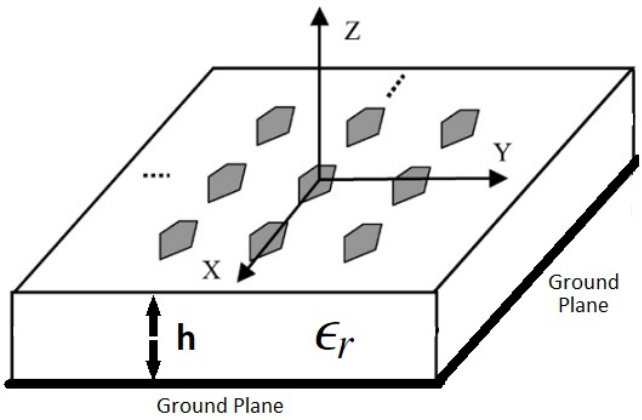

Figure 3.1: A typical periodic structure on a microstrip substrate

In all of the approaches explained in this chapter, DCIM is applied to the reflection coefficients instead of the whole Green's function expression. This is because of the fact that the Green's function is a function of z and z', so the DCIM approximation for the Green's function is valid for fixed values of z and z'. However, when the MoM analysis of periodic dielectric gratings are considered, z and z' parameters need to be varied. Therefore, the DCIM approximation of the reflection coefficients avoids the need for the repetitive complex image calculations for different values of z and z'.

A final note before presenting the approximation procedures and the numerical results is about the choice of the method utilized to extract the coefficients and the exponents of the complex images. In this thesis work, GPOF method is preferred because of its advantage over the Prony method in terms of the sensitivity to numerical noise [19].

3.1 Two-Level Discrete Complex Image Method

3.1.1 Formulation

In this approach, the reflection coefficients R_{TE} and R_q in equation 3.4 are sampled along the path suggested in [24]. This path is shown in Figure 3.2.

The parametric equations describing the paths C_1 and C_2 are as follows:

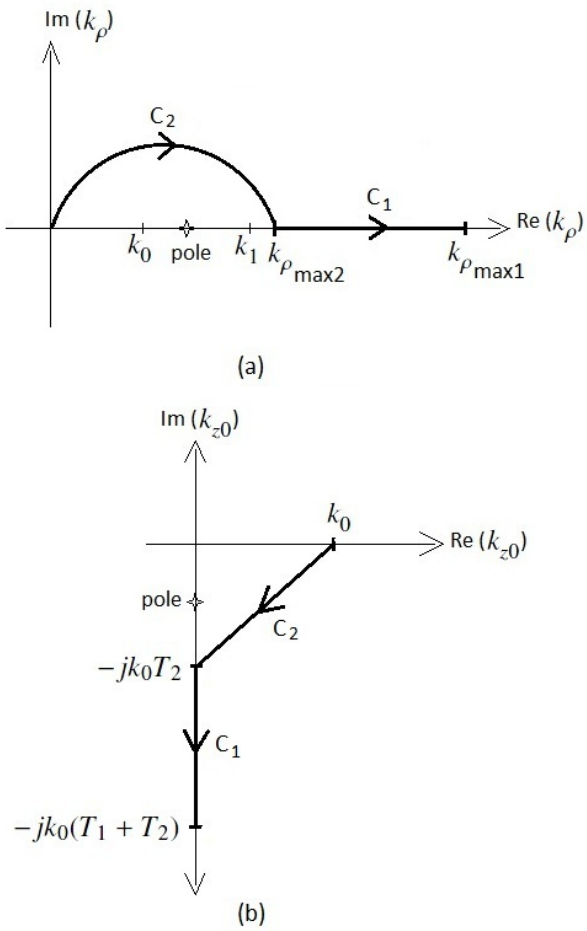

Figure 3.2: The sampling path for 2-Level approach (a) on the complex k_ρ plane and (b) on the complex k_{z0} plane

$$C_1: \quad k_{z0} = -jk_0(T_2 + t) \quad , 0 \le t \le T_1 \tag{3.12}$$

$$C_2: \quad k_{z0} = k_0[-jt + (1 - \frac{t}{T_2})] \quad , 0 \le t \le T_2 \tag{3.13}$$

Recall that, this transformation between k_{z0} and t is necessary for GPOF, because it works only for real variables. T_1 and T_2 are the truncation points for paths C_1 and C_2, respectively. By setting t to these truncation points, we can find $k_{\rho_{max1}}$ and $k_{\rho_{max2}}$:

$$k_{\rho_{max1}} = k_0 \sqrt{1 + (T_1 + T_2)^2} \tag{3.14}$$

$$k_{\rho_{max2}} = k_0 \sqrt{1 + T_2^2} \tag{3.15}$$

The procedure for obtaining the complex image approximation of the periodic Green's function is as follows:

1. Sample $R_1 = R_{TE} + R_q$ along the path C_1 and by using GPOF obtain α_1 and β_1 such that $R_1^{samp} = \sum_{i=1}^{M_1} \alpha_{1i} e^{-jk_{z0}\beta_{1i}}$ for $k_{z0} \in C_1$. M_1 is the number of complex images for approximating the reflection coefficient and it is based on the number of significant singular values obtained in an intermediate stage of the GPOF algorithm.

2. Use α_1 and β_1 along the path C_2 to obtain the effect of the coefficients α_1 and β_1 on the path C_2. That is, find $R_{21}^{samp} = \sum_{i=1}^{M_1} \alpha_{1i} e^{-jk_{z0}\beta_{1i}}$ for $k_{z0} \in C_2$. The subscript 21 means the effect of coefficients of path 1 on path 2.

3. Sample $R_2 = R_{TE} + R_q$ along the path C_2. Subtract R_{21}^{samp} from this sampled reflection coefficient R_2 to obtain R_2^s. By applying GPOF to R_2^s, obtain coefficients α_2 and β_2 such that $R_2^{samp} = \sum_{i=1}^{M_2} \alpha_{2i} e^{-jk_{z0}\beta_{2i}}$ for $k_{z0} \in C_2$. It is not necessary to subtract the effect of the coefficients α_2 and β_2 on the path C_1 from R_1^{samp}, because this effect is very small compared to R_1^{samp}. This fact is verified by numerical experiments.

4. Find $R_1^{app} = \sum_{i=1}^{M_1} \alpha_{1i} e^{-jk_{z0}\beta_{1i}}$ and $R_2^{app} = \sum_{i=1}^{M_2} \alpha_{2i} e^{-jk_{z0}\beta_{2i}}$ and add them to find R_{tot}^{app}. Here, k_{z0} is along the path of the Floquet mode summation. Use R_{tot}^{app} in place of $(R_{TE} + R_q)$ in equation 3.4 to find G_q^{app}. With this G_q^{app} used in place of $\tilde{G}$ in equation 3.1, one can obtain the complex image approximation of the periodic Green's function on the microstrip substrate, G^{app}.

3.1.2 Numerical Results

In this section, the Green's function, G^{app}, obtained by using 2-Level DCIM for reflection coefficients is compared to the exact Green's function, G. The parameters of the structure are given in Table 3.1. The approximation parameters are given in Table 3.2.

Before presenting the results of the comparison between the exact Green's function and the Green's function obtained by 2-level DCIM, it must be made sure that the DCIM is applied succesfully to obtain the complex image representation of the reflection coefficients. For this purpose, the expression $R_{tot}^{app} \frac{e^{-jk_{z0}(z+z')}}{j2k_{z0}}$ is plotted with respect to k_{z0} and compared to the plot

Table 3.1: The parameters of the structure used during the simulations

ϵ_r	dielectric permittivity of the substrate	3.38
h	thickness of the substrate	$0.1\lambda_0$
f	frequency of investigation	30 GHz
a and b	periodicities of the structure	$1.1\lambda_0$
(x', y', z')	coordinates of the source point	(0,0,0)
z	z coordinate of the observation point	0 (on-plane case)
θ	polar angle of the incident wave	π rad

Table 3.2: Approximation parameters of the 2-Level DCIM

T_1	truncation point of the first path	200
N_1	number of samples in the first path	200
T_2	truncation point of the second path	5
N_2	number of samples in the second path	200
M_1	number of complex images used in the first path	7
M_2	number of complex images used in the second path	10

of the expression $(R_{TE} + R_q)\frac{e^{-jk_{z0}(z+z')}}{j2k_{z0}}$ where k_{z0} is along the sampling path instead of the path of the Floquet mode summation. This comparison is shown in Figure 3.3. A good agreement is observed between the complex image representation and the exact values as shown in the figure. The average relative error is in the order of 10^{-6}.

Next, the complex image approximation of the spectral domain Green's function is used in the Floquet mode summation given in equation 3.1 to compute the periodic Green's function at the observation point $\rho = 0.78\lambda_0$ and the results are compared with the exact results with respect to the number of terms used in the summation as seen in Figures 3.4 and 3.5. Exact results refer to the case when the Floquet mode summation is directly applied to the spectral domain Green's function without making any approximations.

Even though, the relative error during the 2-level DCIM approximation was in the order of 10^{-6}, the relative error in the periodic Green's function becomes 10^{-2}. To investigate the possible sources of the error, the approximate spectral domain Green's function is compared with the exact one in Figure 3.6 for real values of k_ρ, since Floquet mode wave numbers k_{xm} and k_{yn}, consequently k_ρ are real.

It can be observed from Figure 3.6 that the complex image approximation obtained by sam-

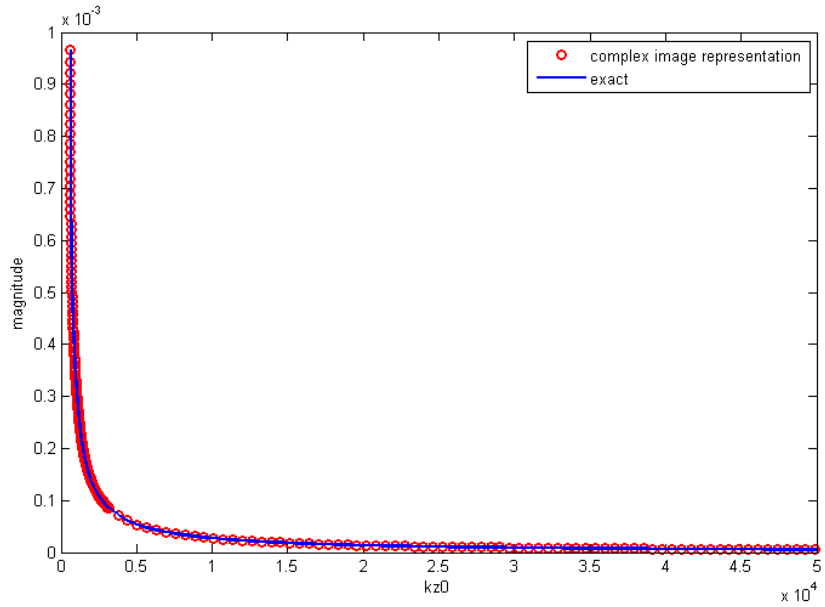

Figure 3.3: Comparison of complex image representation of reflection coefficients obtained by 2-level DCIM to the exact values along the sampling path

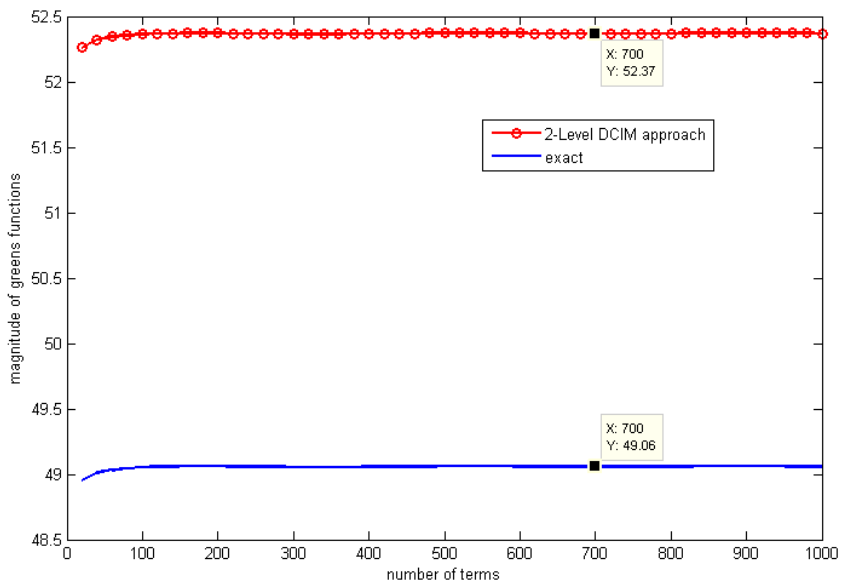

Figure 3.4: Comparison of the approximate (2-Level DCIM) and exact periodic Green's functions at observation point $\rho = 0.78\lambda_0$

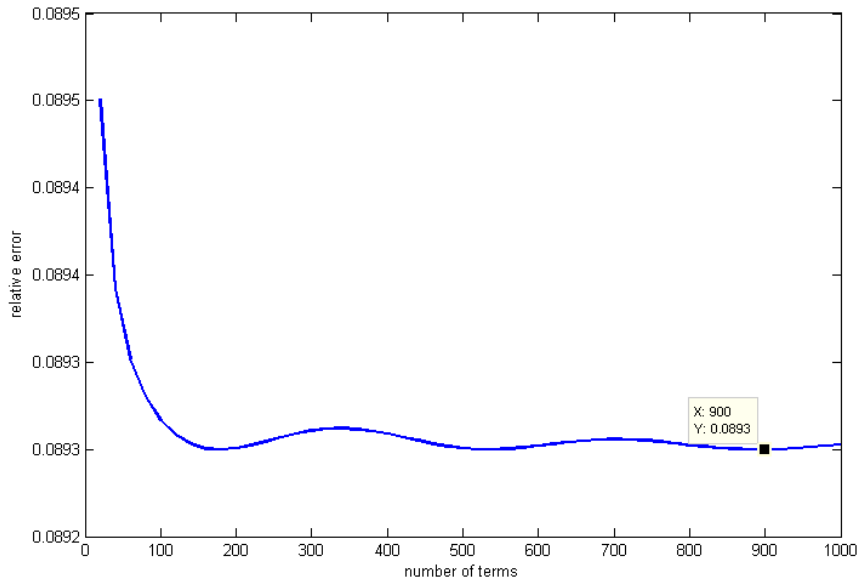

Figure 3.5: Relative error between the approximate (2-Level DCIM) and the exact periodic Green's functions at observation point $\rho = 0.78\lambda_0$

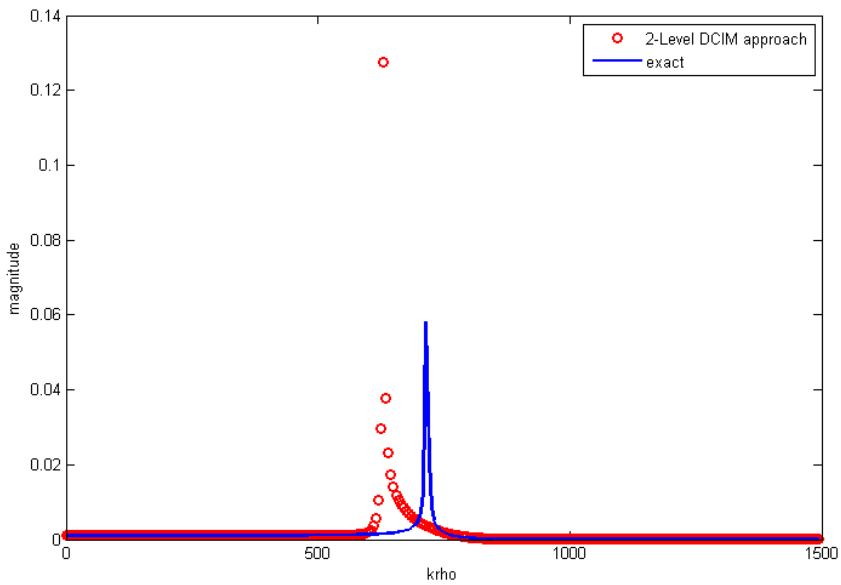

Figure 3.6: Comparison of approximate (2-Level DCIM) and exact spectral domain Green's functions along the real axis of the $k_\rho - plane$

pling the spectral domain Green's function along the path C_2, that corresponds to complex values of k_ρ, does not accurately model the contribution of the surface wave pole along the real axis of the $k_\rho - plane$. This discrepancy does not cause a problem for the evaluation of the spatial domain Green's function for a single source with DCIM since the integral of the complex image approximation along C_1 and C_2 and the integral of the exact Green's function along the real axis of $k_\rho - plane$ give same results. However, for the periodic case, there is a Floquet mode summation instead of an inverse Fourier transform integral for the transformation from the spectral domain to the spatial domain. Therefore, each term of the summation should be accurately approximated for the accuracy of the end result which is the spatial domain Green's function. From this observation, it is clear that surface wave contributions need to be extracted.

3.2 Two-Level Discrete Complex Image Method with Surface Wave Pole Extraction

3.2.1 Formulation

The formulation for this approach is the same as that of the 2-Level DCIM approach except that the contributions of the surface wave poles are extracted prior to sampling. Recall that the contribution of the SWP can be written in the following form in the spectral domain:

$$\tilde{G}_{sw} = \frac{2k_{\rho p} Res}{k_\rho^2 - k_{\rho p}^2} \tag{3.16}$$

where $k_{\rho p}$ is the surface wave pole and Res is its residue. In order to compute the residue of the pole, the following theorem from complex calculus is utilized [41]:

If $f(z)$ and $g(z)$ are analytic at z_0, and if $g(z)$ has a simple zero at z_0, then

$$Res\left[\frac{f(z)}{g(z)}, z_0\right] = \frac{f(z_0)}{g'(z_0)} \tag{3.17}$$

The derivative operation is performed numerically by using first order finite difference formulas. After finding the surface wave pole ($k_{\rho p}$) and the residue for that pole (Res), the procedure described in section 3.1 is applied with the difference being that the expression in 3.16 is subtracted from the reflection coefficients $R_1 = R_{TE} + R_q$ and $R_2 = R_{TE} + R_q$ and the procedure

is continued with these new values for R_1 and R_2. The complex image contribution, G_{ci}^{app} is obtained by this procedure, but to find the total G^{app}, one must add the contribution of the surface wave pole. This contribution is found simply by putting the expression in 3.16 in place of $(R_{TE} + R_q)$ in equation 3.4 to find G_q^{sw}. With this G_q^{sw} used in place of $\tilde{G}$ in equation 3.1, the contribution from the surface wave, G_{sw}^{app} is obtained.

3.2.2 Numerical Results

The structure whose parameters are given in Table 3.1 is also studied in this section. The approximation parameters of the DCIM are given in Table 3.3.

Table 3.3: Approximation parameters for 2-Level DCIM with SW Extraction Approach

T_1	200
N_1	200
T_2	5
N_2	200
M_1	7
M_2	7

In order to investigate whether the extraction of surface wave pole contribution helps the DCIM model the contribution of the surface wave pole correctly, approximate spectral domain Green's function is compared with the exact one in Figure 3.7 for real values of k_ρ. Since, the discrepancy is small for this case, the relative error plot is also shown in Figure 3.8.

As observed in Figure 3.8, by extracting the surface wave contributions, the error introduced by the DCIM is significantly reduced. In order to investigate the effects of SW extraction on the accuracy of the periodic Green's function, the magnitudes of the approximate and exact periodic Green's functions are compared in Figure 3.9. The relative error values are also plotted in Figure 3.10.

It can be observed that the error is reduced to a level of 10^{-4} by extracting the surface wave contributions. Even though the accuracy is improved significantly, the 3-level approximation scheme, where the sampling of the spectral domain Green's function is performed along the real k_ρ axis, is also studied in order to explore the possibility of reducing the error even further.

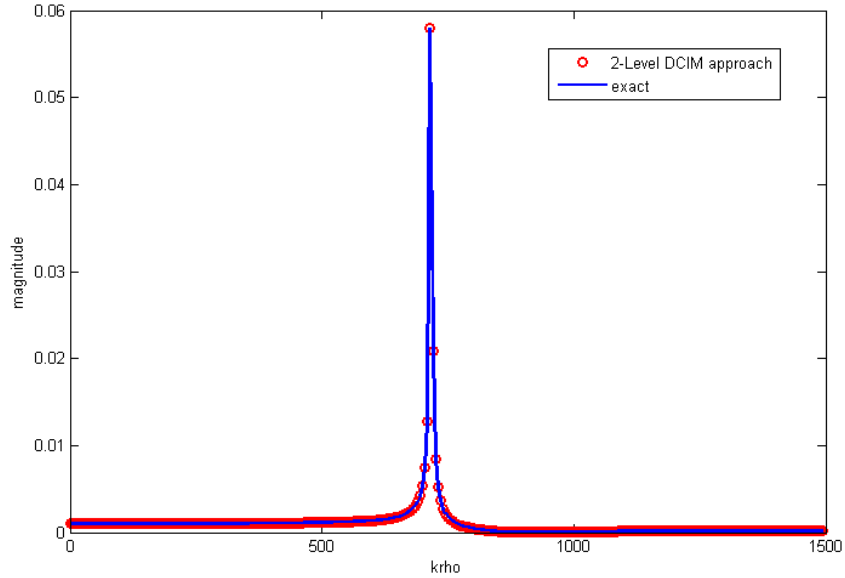

Figure 3.7: Comparison of approximate (2-Level DCIM with surface wave extraction) and exact spectral domain Green's functions along the real axis of the $k_\rho - plane$

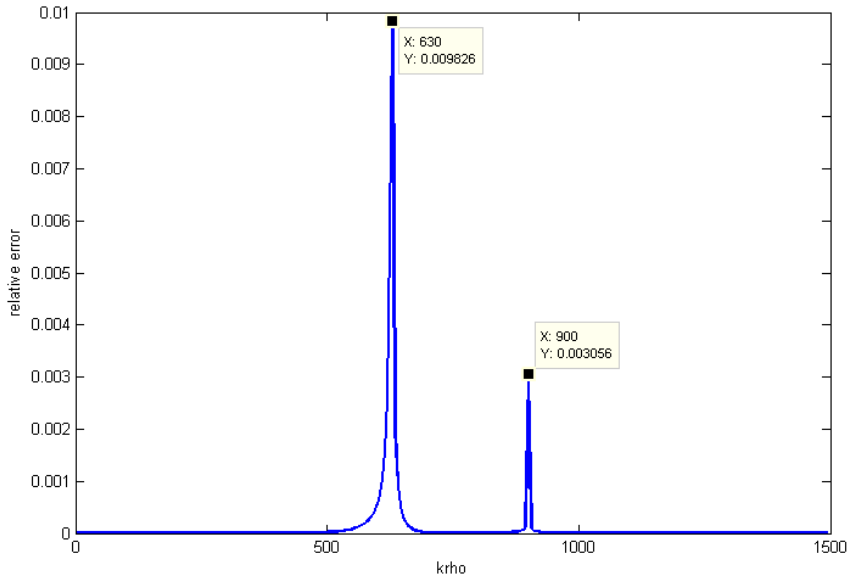

Figure 3.8: Relative error between the approximate (2-Level DCIM with surface wave extraction) and exact spectral domain Green's functions along the real axis of the $k_\rho - plane$

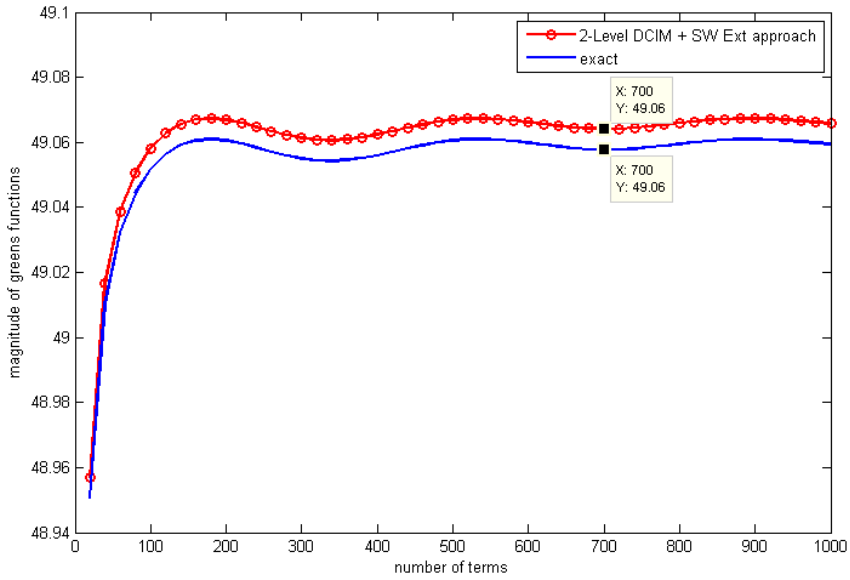

Figure 3.9: Comparison of the approximate (2-Level DCIM with surface wave extraction) and exact periodic Green's functions at observation point $\rho = 0.78\lambda_0$

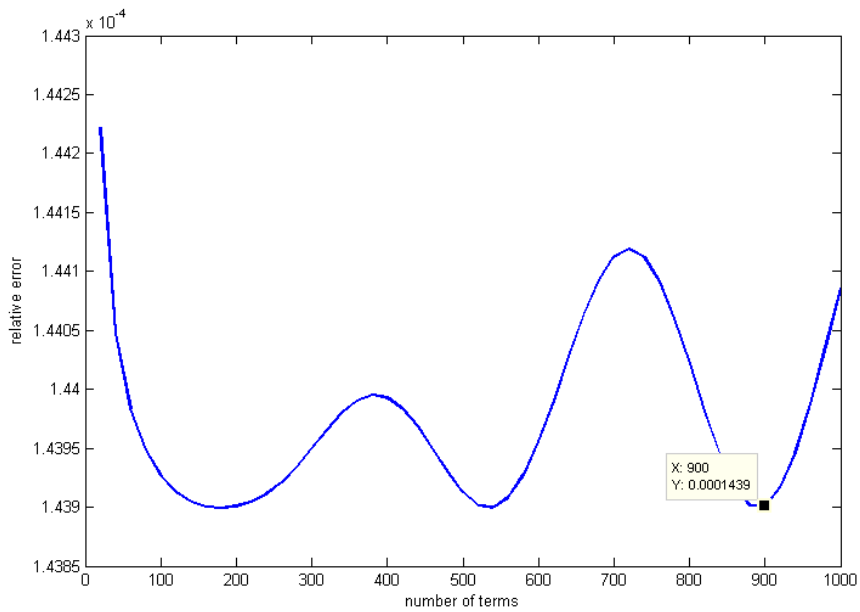

Figure 3.10: Relative error between the approximate (2-Level DCIM with surface wave extraction) and the exact periodic Green's functions at observation point $\rho = 0.78\lambda_0$

3.3 Three-Level Discrete Complex Image Method with Surface Wave Pole Extraction

3.3.1 Formulation

In this approach, the reflection coefficients R_{TE} and R_q in equation 3.4 are sampled along the real axis of $k_\rho - plane$ as suggested in [27]. This path is shown in Figure 3.11.

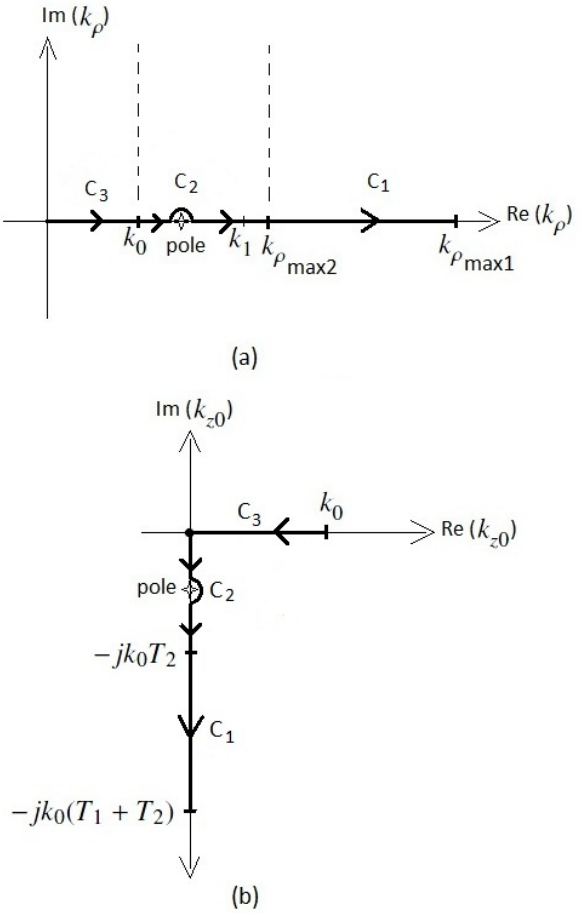

Figure 3.11: The sampling path for 3-Level approach (a) on the complex k_ρ plane and (b) on the complex k_{z0} plane

The parametric equations describing the paths C_1, C_2 and C_3 are as follows:

$$C_1: \quad k_{z0} = -jk_0(T_2 + t) \quad , 0 \leq t \leq T_1 \tag{3.18}$$

$$C_2: \quad k_{z0} = -jk_0 t \quad , 0 \leq t \leq T_2 \tag{3.19}$$

$$C_3: \quad k_{z0} = k_0(1 - t) \quad , 0 \leq t \leq 1 \tag{3.20}$$

Since the endpoints of path C_3 is already defined (0 and k_0), we only need to enter the number of samples for that path. The expressions for $k_{\rho_{max1}}$ and $k_{\rho_{max2}}$ are same as in 2-Level approach (equations 3.14 and 3.15).

The procedure of this approach for obtaining the complex image approximation of the periodic Green's function is as follows:

1. Sample $R_1 = R_{TE} + R_q$ after subtracting the expression in equation 3.16 from it along the path C_1 and by using GPOF obtain α_1 and β_1 such that $R_1^{samp} = \sum_{i=1}^{M_1} \alpha_{1i} e^{-jk_{z0}\beta_{1i}}$ for $k_{z0} \in C_1$.

2. Use α_1 and β_1 along the path C_2 to obtain the effect of the coefficients α_1 and β_1 on the path C_2. That is, find $R_{21}^{samp} = \sum_{i=1}^{M_1} \alpha_{1i} e^{-jk_{z0}\beta_{1i}}$ for $k_{z0} \in C_2$.

3. Use α_1 and β_1 along the path C_3 to obtain the effect of the coefficients α_1 and β_1 on the path C_3. That is, find $R_{31}^{samp} = \sum_{i=1}^{M_1} \alpha_{1i} e^{-jk_{z0}\beta_{1i}}$ for $k_{z0} \in C_3$.

4. Sample $R_2 = R_{TE} + R_q$ after subtacting the expression in equation 3.16 from it along the path C_2. Subtract R_{21}^{samp} from this sampled reflection coefficient R_2 to obtain R_2^s. By applying GPOF to R_2^s, obtain coefficients α_2 and β_2 such that $R_2^{samp} = \sum_{i=1}^{M_2} \alpha_{2i} e^{-jk_{z0}\beta_{2i}}$ for $k_{z0} \in C_2$.

5. Use α_2 and β_2 along the path C_3 to obtain the effect of the coefficients α_2 and β_2 on the path C_3. That is, find $R_{32}^{samp} = \sum_{i=1}^{M_1} \alpha_{2i} e^{-jk_{z0}\beta_{2i}}$ for $k_{z0} \in C_3$.

6. Sample $R_3 = R_{TE} + R_q$ after subtacting the expression in equation 3.16 from it along the path C_3. Subtract R_{31}^{samp} and R_{32}^{samp} from this sampled reflection coefficient R_3 to obtain R_3^s. By applying GPOF to R_3^s, obtain coefficients α_3 and β_3 such that $R_3^{samp} = \sum_{i=1}^{M_3} \alpha_{3i} e^{-jk_{z0}\beta_{3i}}$ for $k_{z0} \in C_3$.

7. Find $R_1^{app} = \sum_{i=1}^{M_1} \alpha_{1i} e^{-jk_{z0}\beta_{1i}}$, $R_2^{app} = \sum_{i=1}^{M_2} \alpha_{2i} e^{-jk_{z0}\beta_{2i}}$ and $R_3^{app} = \sum_{i=1}^{M_3} \alpha_{3i} e^{-jk_{z0}\beta_{3i}}$ and add them to find R_{tot}^{app}. Here, k_{z0} is along the path of the Floquet mode summation. Use this in place of $(R_{TE} + R_q)$ in equation 3.4 to find G_q^{app}. With this G_q^{app} used in place of $\tilde{G}$ in equation 3.1, one can obtain the complex image approximation of the periodic Green's function on the microstrip substrate, G^{app}.

3.3.2 Numerical Results

The approximation parameters used during the 3-level DCIM are given in Table 3.4.

Table 3.4: Approximation parameters for 3-Level DCIM Approach

T_1	truncation point of the first path	200
N_1	number of samples in the first path	200
T_2	truncation point of the second path	5
N_2	number of samples in the second path	200
N_3	number of samples in the third path	50
M_1	number of complex images used in the first path	8
M_2	number of complex images used in the second path	5
M_3	number of complex images used in the third path	5

The accuracy of the modeling of the surface wave contribution by DCIM is investigated by comparing the approximate spectral domain Green's function with the exact one for real values of k_ρ. The relative error plot is shown in Figure 3.12.

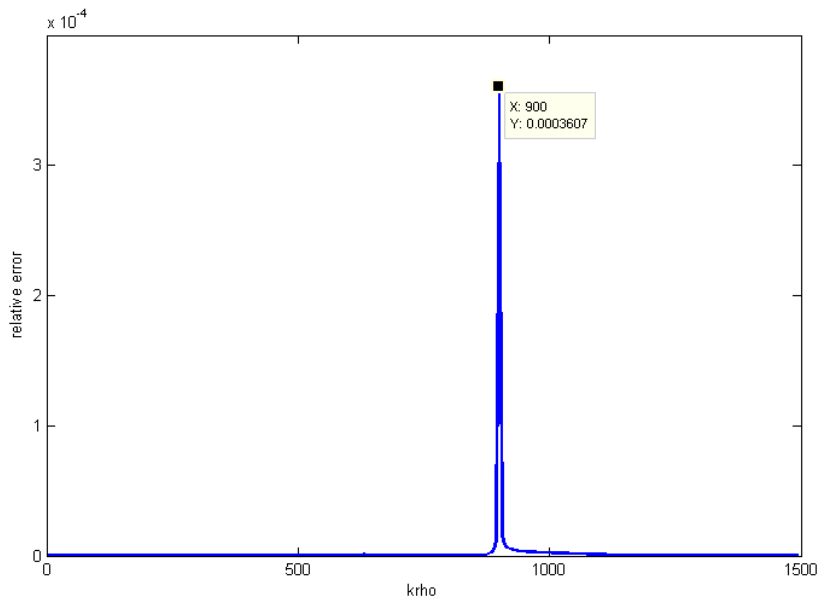

Figure 3.12: Relative error between the approximate (3-Level DCIM with surface wave extraction) and exact spectral domain Green's functions along the real axis of the $k_\rho - plane$

As observed in Figure 3.12, the relative error is reduced to the levels of 10^{-4}. In order to investigate the effects of this reduction on the accuracy of the periodic Green's function, the

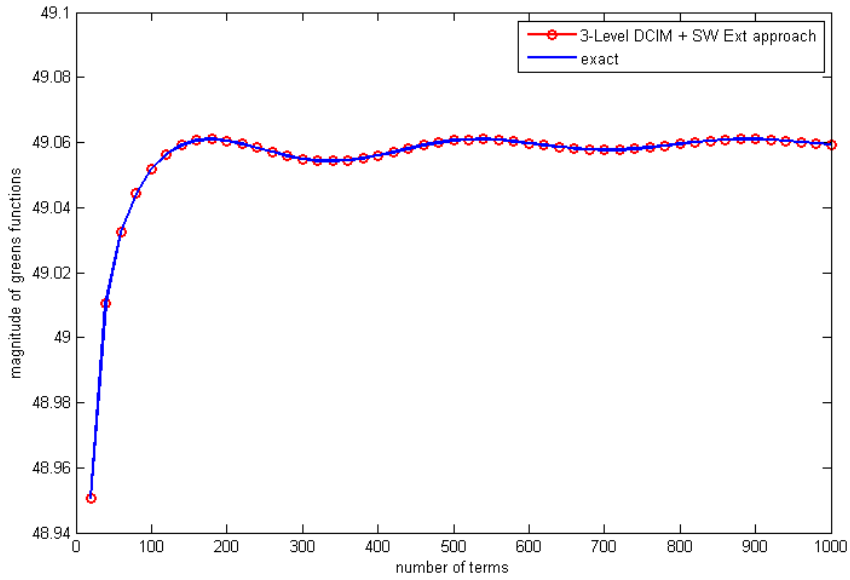

Figure 3.13: Comparison of the approximate (3-Level DCIM with surface wave extraction) and exact periodic Green's functions at observation point $\rho = 0.78\lambda_0$

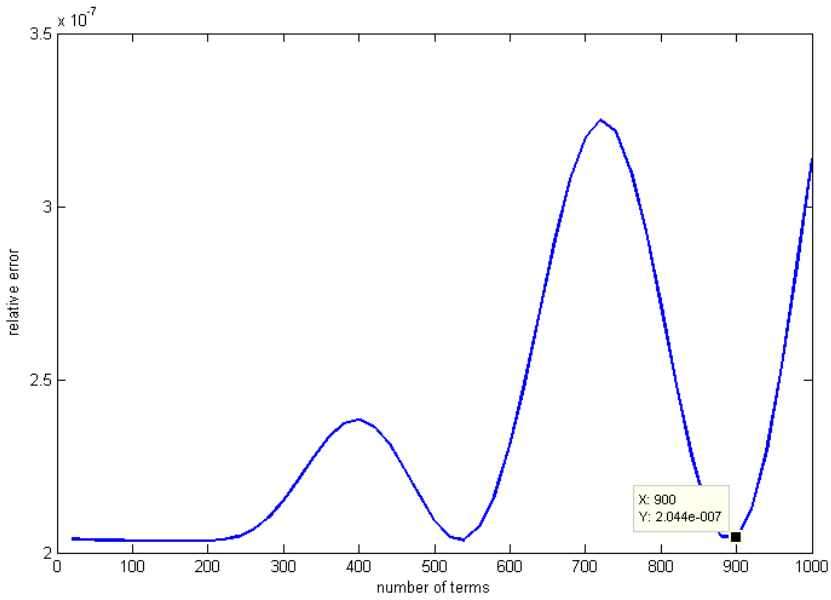

Figure 3.14: Relative error between the approximate (3-Level DCIM with surface wave extraction) and the exact periodic Green's functions at observation point $\rho = 0.78\lambda_0$

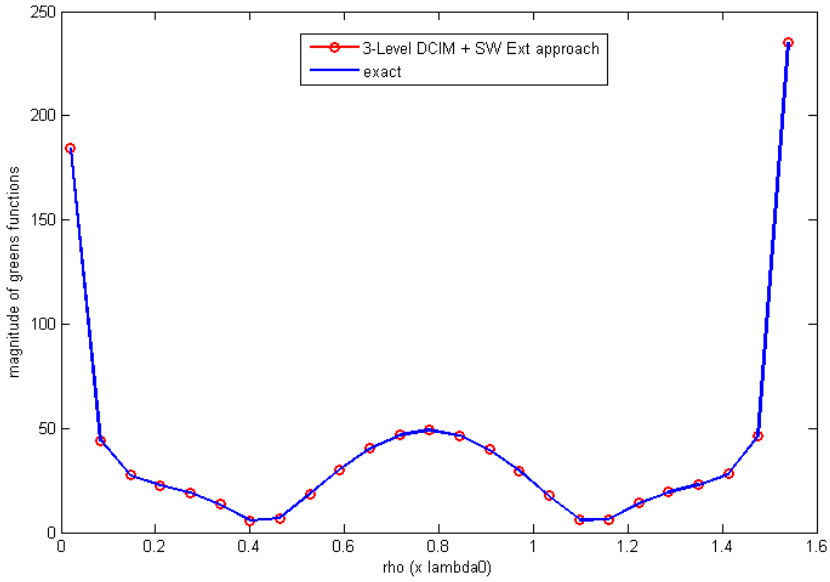

Figure 3.15: Magnitudes of the approximate (3-Level DCIM with surface wave extraction) and exact periodic Green's functions at observation points along the diagonal of a unit cell

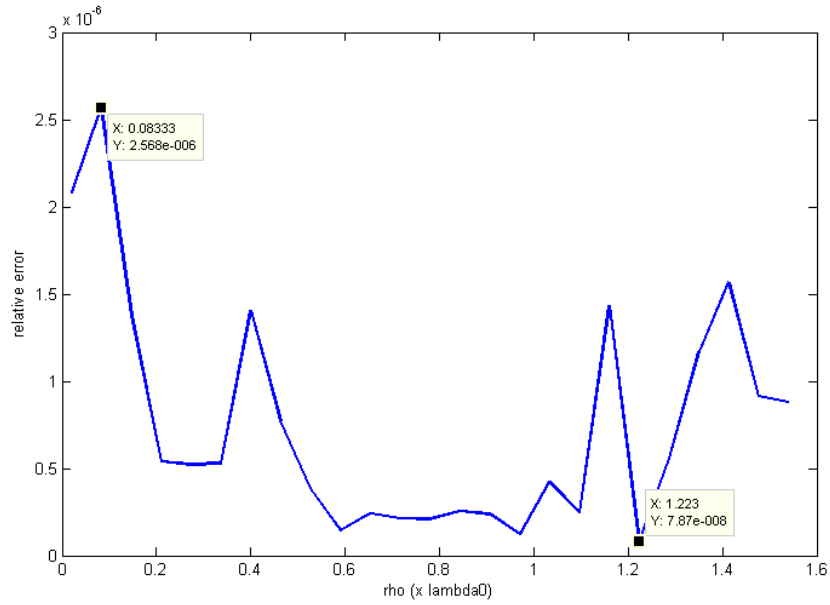

Figure 3.16: Relative error between the approximate (3-Level DCIM with surface wave extraction) and exact periodic Green's functions at observation points along the diagonal of a unit cell

magnitudes of the approximate and exact periodic Green's functions are compared in Figure 3.13. The relative error values are also plotted in Figure 3.14. As can be seen in the figure, the relative error values have decreased to the levels of 10^{-7}.

The behaviour of the periodic Green's function with respect to the location of the observation point is observed by plotting the magnitudes of the approximate and exact Green's functions for along the diagonal of a unit cell. This plot is shown in Figure 3.15. Since in the application of MoM, the Green's functions are integrated with the source functions to obtain the matrix entries, the level of the relative error at each observation point is crucial. For this reason, the relative error is plotted against the observation points along the diagonal of a unit cell, to investigate the limits of the relative error. This plot is shown in Figure 3.16. Note that, in this simulation, the Floquet mode summations are truncated at 1001×1001 terms.

The 3-level DCIM with surface wave extraction has reduced the average relative error between the exact periodic Green's function in layered media and the complex image approximation of it to the levels of 10^{-7}. The next task of this thesis work is to accelerate the computation of the series representing this Green's function, which is handled in the next chapter.

CHAPTER 4

ACCELERATING THE COMPUTATION OF THE SERIES REPRESENTING THE PERIODIC GREEN'S FUNCTION IN LAYERED MEDIA

In this chapter, the work done for accelerating the computation of the Green's function is explained. The Green's function expression to be accelerated is the one obtained by using 3-Level DCIM Approach (see Section 3.3), since it gives the most accurate results. First, the formulation of the problem is given and then the numerical results are presented.

4.1 Formulation

The Green's function expression obtained by using 3-Level DCIM Approach is given as :

$$G = \frac{1}{ab} \sum_{m=-\infty}^{\infty} \sum_{n=-\infty}^{\infty} \tilde{G}_q^{app} e^{-jk_{xm}(x-x')} e^{-jk_{yn}(y-y')} \tag{4.1}$$

where $\tilde{G}_q^{app}$ is given as:

$$\tilde{G}_q^{app} = \frac{1}{j2k_{z0}} [e^{-jk_{z0}(z-z')} + R_{tot}^{app} e^{-jk_{z0}(z+z')}] \tag{4.2}$$

Here, R_{tot}^{app} is the total approximated reflection coefficient consisting of R_1^{app}, R_2^{app} and R_3^{app}. When we put the expression for $\tilde{G}_q^{app}$ in equation 4.1 we see that the periodic Green's function can be considered as the sum of a direct term (G^{dir}) and a reflected term (G^{ref}):

$$G^{dir} = \frac{1}{ab}\sum_{m=-\infty}^{\infty}\sum_{n=-\infty}^{\infty}\frac{e^{-jk_{z0}(z-z')}}{j2k_{z0}}e^{-jk_{xm}(x-x')}e^{-jk_{yn}(y-y')} \tag{4.3}$$

$$G^{ref} = \frac{1}{ab}\sum_{m=-\infty}^{\infty}\sum_{n=-\infty}^{\infty}R_{tot}^{app}\frac{e^{-jk_{z0}(z+z')}}{j2k_{z0}}e^{-jk_{xm}(x-x')}e^{-jk_{yn}(y-y')} \tag{4.4}$$

It is seen that G^{dir} is exactly the same as equation 2.22 which is the expression for free space periodic Green's function (FSPGF). Thus, the formulation for the application of the Ewald Method to this term is exactly the same as described in Section 2.3.

The reflected term of the periodic Green's function can be further split into three parts, namely $G^{ref,1}$, $G^{ref,2}$ and $G^{ref,3}$ since R_{tot}^{app} is the sum of R_1^{app}, R_2^{app} and R_3^{app}. The expressions for these three approximated reflection coefficients were given in Section 3.3 and they are repeated here:

$$R_1^{app} = \sum_{i=1}^{M_1}\alpha_{1i}e^{-jk_{z0}\beta_{1i}} \tag{4.5}$$

$$R_2^{app} = \sum_{i=1}^{M_2}\alpha_{2i}e^{-jk_{z0}\beta_{2i}} \tag{4.6}$$

$$R_3^{app} = \sum_{i=1}^{M_3}\alpha_{3i}e^{-jk_{z0}\beta_{3i}} \tag{4.7}$$

By putting these expressions in place of R_{tot}^{app} in equation 4.4, we obtain $G^{ref,1}$, $G^{ref,2}$ and $G^{ref,3}$. Since the expressions for these three terms are very similar, the Ewald formulation will be given only for the first part. $G^{ref,1}$ is given as follows:

$$G^{ref,1} = \frac{1}{ab}\sum_{m=-\infty}^{\infty}\sum_{n=-\infty}^{\infty}\sum_{i=1}^{M_1}\alpha_{1i}\frac{e^{-jk_{z0}(z+z'+\beta_{1i})}}{j2k_{z0}}e^{-jk_{xm}(x-x')}e^{-jk_{yn}(y-y')} \tag{4.8}$$

When the equation 4.8 is observed, one can realize that it is in the same form as equation 2.22 with some differences. There is an extra summation $\sum_{i=1}^{M_1}$ and an extra factor α_{1i}. Also, $z - z'$ terms are replaced with $z + z' + \beta_{1i}$. By making these changes, the Ewald summation for this reflected term is obtained as:

$$G_1^{ref,1} = \frac{1}{4ab}\sum_{m=-\infty}^{\infty}\sum_{n=-\infty}^{\infty}\sum_{i=1}^{M_1}\alpha_{1i}\frac{e^{-j[k_{xm}(x-x')+k_{yn}(y-y')]}}{jk_{z0}}\sum_{\pm}e^{\pm jk_{z0}(z+z'+\beta_{1i})}erfc\left(\frac{jk_{z0}}{2E}\pm(z+z'+\beta_{1i})E\right) \tag{4.9}$$

$$G_2^{ref,1} = \frac{1}{8\pi} \sum_{m=-\infty}^{\infty} \sum_{n=-\infty}^{\infty} \sum_{i=1}^{M_1} \alpha_{1i} \frac{e^{-j(k_x^i ma + k_y^i nb)}}{R_{1i}} \sum_{\pm} e^{\pm jk_0 R_{1i}} erfc(R_{1i}E \pm \frac{jk_0}{2E}) \tag{4.10}$$

with E being the Ewald splitting parameter and R_{1i} being the complex distance given as:

$$R_{1i} = \sqrt{(x - x' - ma)^2 + (y - y' - nb)^2 + (z + z' + \beta_{1i})^2} \tag{4.11}$$

$G_1^{ref,1}$ and $G_2^{ref,1}$ are combined to get Ewald summation for $G^{ref,1}$, ($G_{ew}^{ref,1}$). By the same way, $G_{ew}^{ref,2}$ and $G_{ew}^{ref,3}$ are obtained. These three are summed together to get G_{ew}^{ref}. The expression for G_{ew}^{dir} is already known from Section 2.3. G_{ew}^{ref} and G_{ew}^{dir} are added together to obtain G_{ew}, the Ewald summation for the periodic Green's function in the microstrip structure.

Note that the Ewald method decomposes the periodic Green's function into two parts; G_1 and G_2. Since the equation 4.9 is a spectral summation, it is sometimes referred to as 'spectral series' while the equation 4.10 is referred to as 'spatial series' since it is a spatial summation.

The Ewald method discussed up to now is applied only to the part of the Green's function that is approximated by complex exponentials. The surface wave contributions, on the other hand, are not expressed as exponentials. The spatial domain contribution of the surface wave poles for periodic structures can be expressed in terms of a spatial summation as:

$$G_{sw}^{periodic} = \sum_{m=-\infty}^{\infty} \sum_{n=-\infty}^{\infty} -\frac{j}{2}(Res) H_0^{(2)}(k_{\rho p}\rho) k_{\rho p} e^{-jk_x^i ma} e^{-jk_y^i nb} \tag{4.12}$$

The Ewald method is extended to the summations in the form of equation 4.12 in [44]. In this thesis work, this method is not applied and the surface wave contributions are found by spectral summation without any approximation method. For this reason, the details of the method presented in [44] are not discussed here. The acceleration of the series representing the contributions of the surface wave poles in periodic structures is considered to be a future work.

The convergence of the spectral summation for the surface wave contribution is investigated for the observation point $\rho = 0.78\lambda_0$ and plotted in Figure 4.1

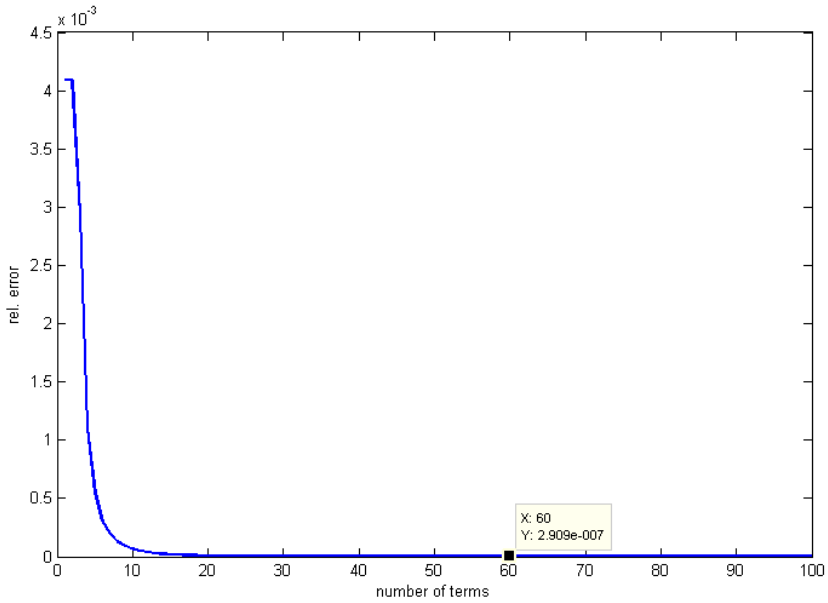

Figure 4.1: Convergence of the spectral summation for the surface wave contribution

4.2 Numerical Results

In this section, the results for the Ewald's Method is presented. The complementary error functions $erfc$ in the Ewald summation expressions contain complex values inside their arguments. The extension of the error function to the complex plane is described in [42]. This document and the implementation of it for Matlab (an M-file) can be found at the website [43].

The approximation parameters used for the 3-Level DCIM approach is same as in the previous chapter. Another approximation parameter in the simulations is the Ewald splitting parameter, E. First, we will investigate the effect of this parameter to the convergence rate of both the spectral series and the spatial series. For $E = 0.7E_{opt}$, the convergence of the spectral and spatial series are shown in Figures 4.2 and 4.3, respectively. For $E = E_{opt}$, the plots are given in Figures 4.4 and 4.5 while the convergence rates for $E = 1.6E_{opt}$ are shown in Figures 4.6 and 4.7 Note that, this investigation is done for the direct term of the Green's function for the sake of simplicity.

It is observed that as the Ewald splitting parameter increases, the spectral series converges more slowly while the convergence rate of the spatial series increases. The reason for this

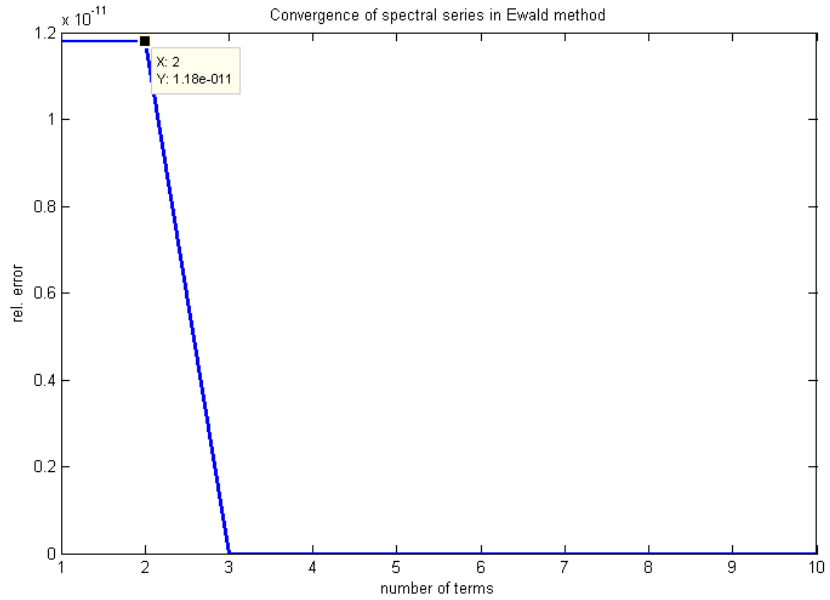

Figure 4.2: Convergence of the spectral series of Ewald summation for $E = 0.7E_{opt}$

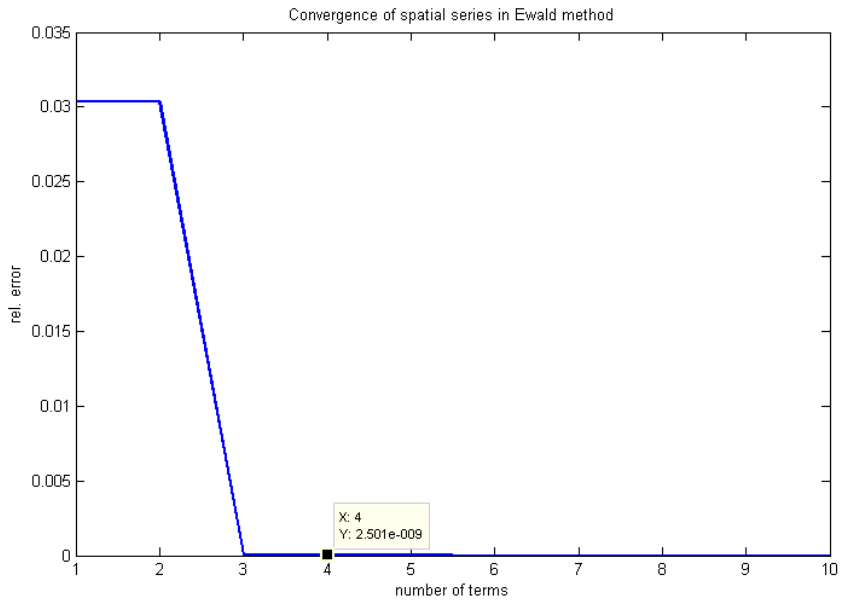

Figure 4.3: Convergence of the spatial series of Ewald summation for $E = 0.7E_{opt}$

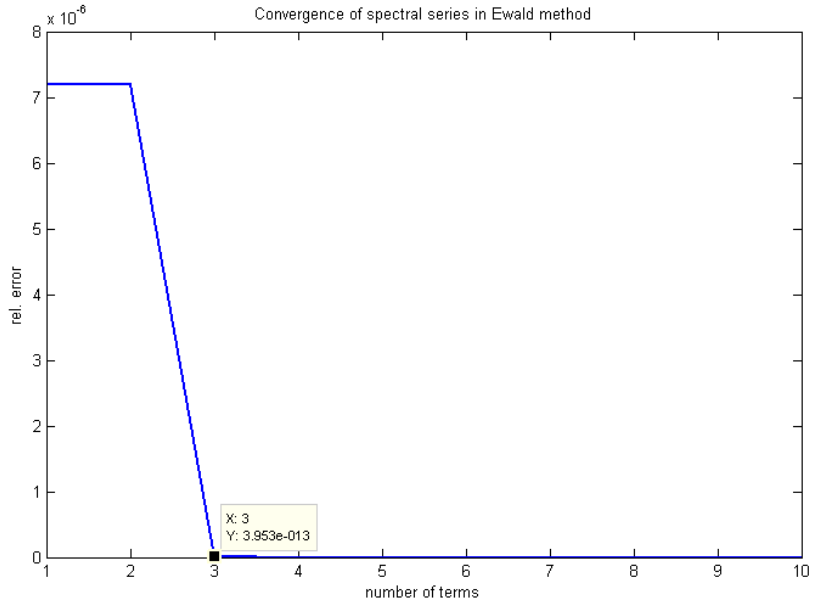

Figure 4.4: Convergence of the spectral series of Ewald summation for $E = E_{opt}$

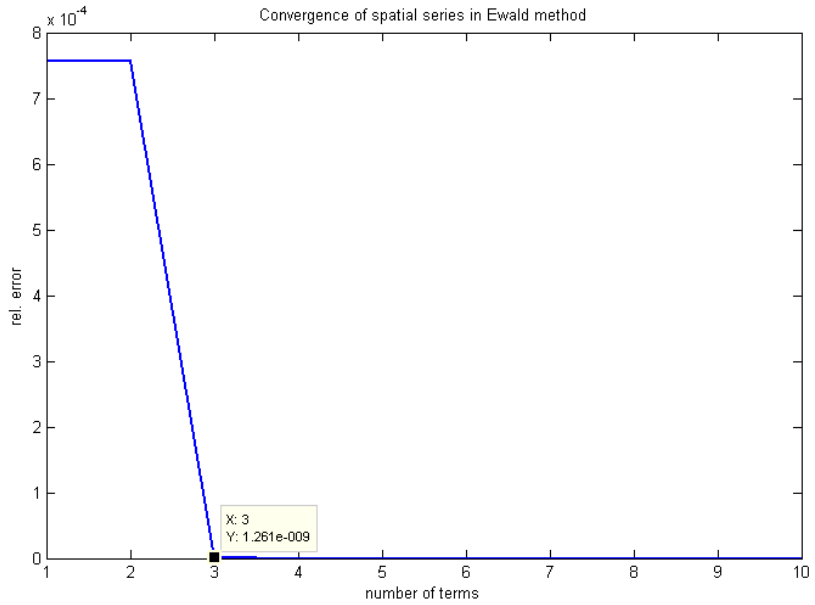

Figure 4.5: Convergence of the spatial series of Ewald summation for $E = E_{opt}$

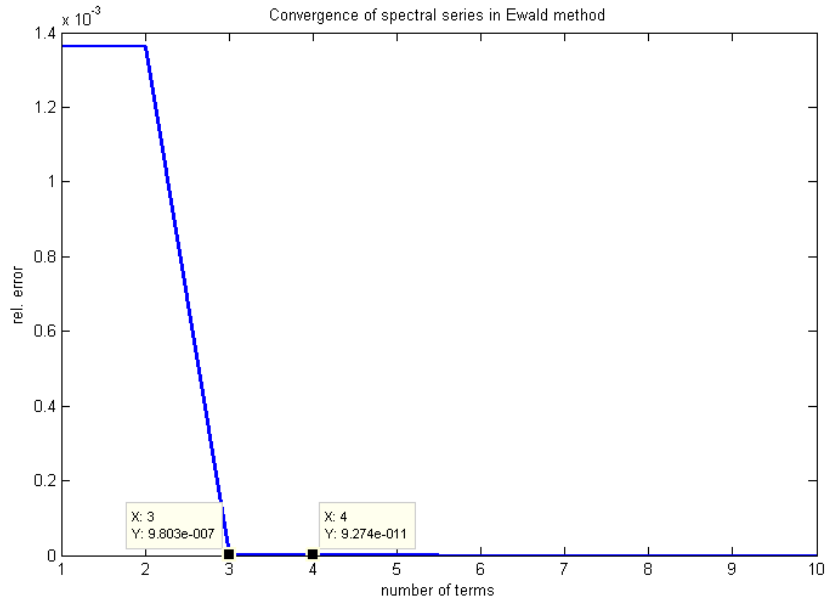

Figure 4.6: Convergence of the spectral series of Ewald summation for $E = 1.6E_{opt}$

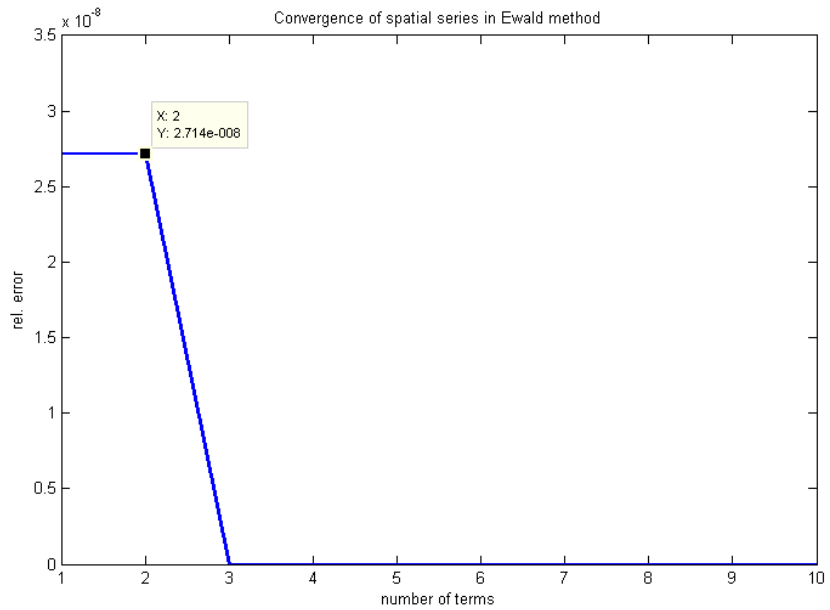

Figure 4.7: Convergence of the spatial series of Ewald summation for $E = 1.6E_{opt}$

becomes clear when we analyze equations 2.29 and 2.30. The Ewald splitting parameter defines the upper limit of the integral in spectral part while it determines the lower limit in spatial part. For these parameters of the structure, the best overall convergence rate is obtained when $E = E_{opt}$. In that case, the number of terms used in Ewald summation is the same for both the spectral and spatial series. Thus, $E = E_{opt}$ is used in the simulations for these parameters of the structure. Next, the convergence rates of the series summations for the direct and the reflected term are investigated with $E = E_{opt}$. For this value of the Ewald splitting parameter, the convergence of the series representing the direct term is shown in the Figures 4.4 and 4.5. The convergence of the series representing the reflected term of the periodic Green's function is shown in Figure 4.8

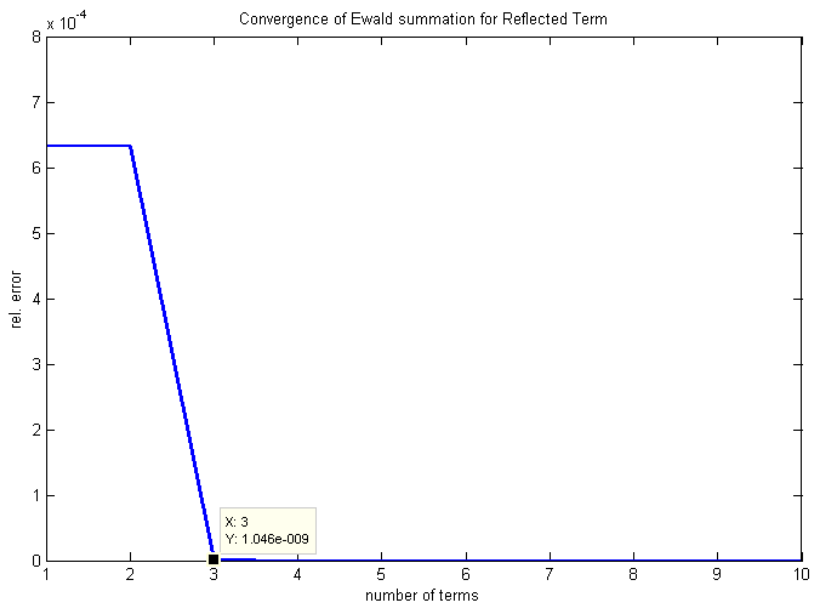

Figure 4.8: Convergence of Ewald summation for the reflected term of the Green's function

After determining the number of terms needed for Ewald summation, we use those numbers for summation and compare the results to that of exact spectral summation. These plots are shown in Figures 4.9. From this figure, one can conclude that the result of the exact spectral summation oscillates near a final value and converge to it very slowly while the Ewald summation reaches to that final value with a very small term number.

The CPU time for the Ewald summation is 0.225 seconds and for surface wave contribution summation it is 0.020 seconds while for the direct spectral summation, the time needed is

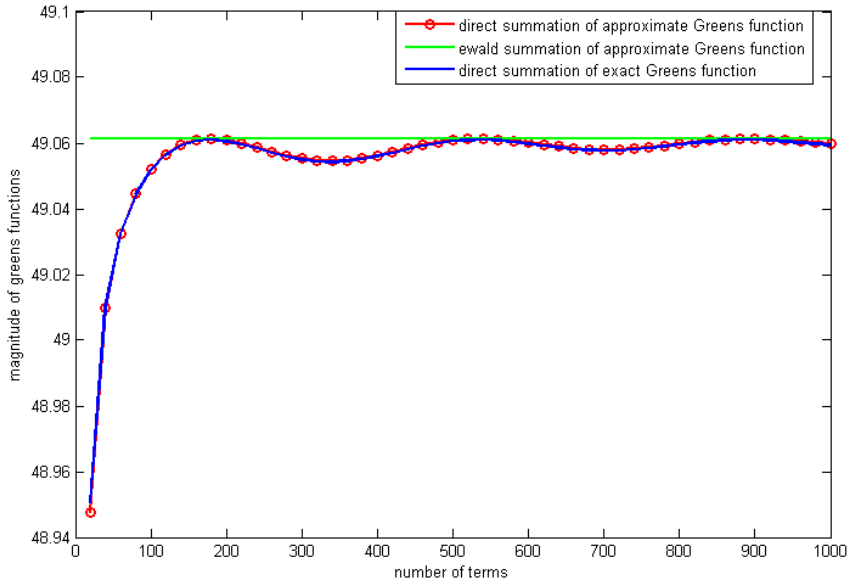

Figure 4.9: Comparison of the approximate Green's function accelerated by Ewald summation with approximate and exact Green's functions with no acceleration

161.44 seconds. Note that, the CPU time measured for direct spectral summation is the time for 5001×5001 terms and this number of terms is still not enough for it to converge.

Next, the effect of the periodicity of the structure (a and b) on the accuracy of the Ewald summation is investigated. For this purpose, a and b are increased to $4.3\lambda_0$ and the direct term of the Green's functon is computed by Ewald's method. The convergences of the spectral and the spatial series are shown in Figures 4.10 and 4.11. Both series converges with 7×7 terms. (The number of terms seen in the figures are the number of terms at one half of a side of the structure.) The spectral series converges to $-6.137471214487152 \times 10^{23} + j3.755745845781550 \times 10^{8}$ while the spatial series converges to $6.137471214487246 \times 10^{23} - j1.934323331365723 \times 10^{8}$. The total series converges to the sum of these numbers which is $9.395240960000000 \times 10^{9} + j1.821422514415827 \times 10^{8}$.The reason for these huge values and consequently the loss of accuracy is described in Section 2.3.

The remedy for the problem of accuracy loss is to increase the Ewald splitting parameter, E beyond E_{opt}. Therefore, E is set to $2E_{opt}$ and the direct term of the Green's function is computed again by Ewald's method. For this new value of the splitting parameter, the spectral series converges to $-3.709872057975033 \times 10^{5} + j9.017734101038753$ while the spatial series converges to $3.709928913770443 \times 10^{5} - j8.606354363519641 \times 10^{-14}$. As

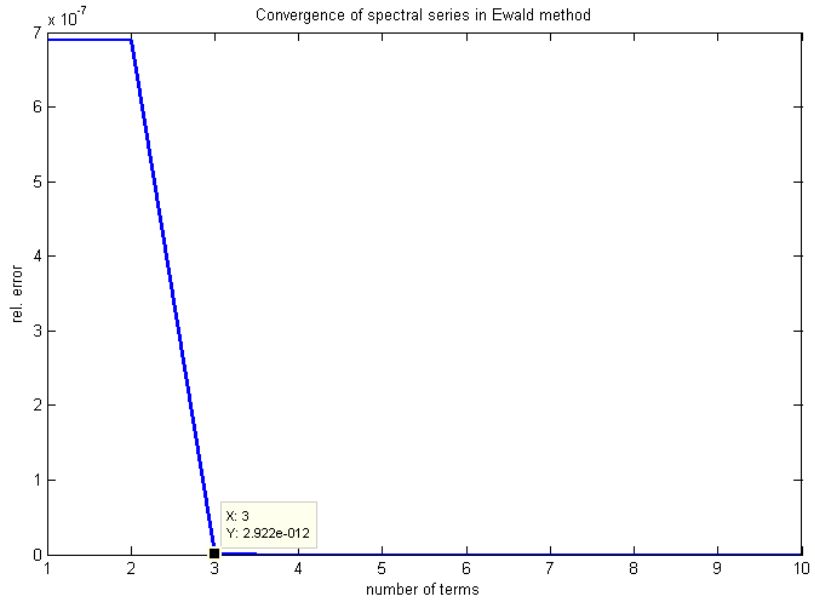

Figure 4.10: Convergence of the spectral series of Ewald summation for $a = b = 4.3\lambda_0$ and $E = E_{opt}$

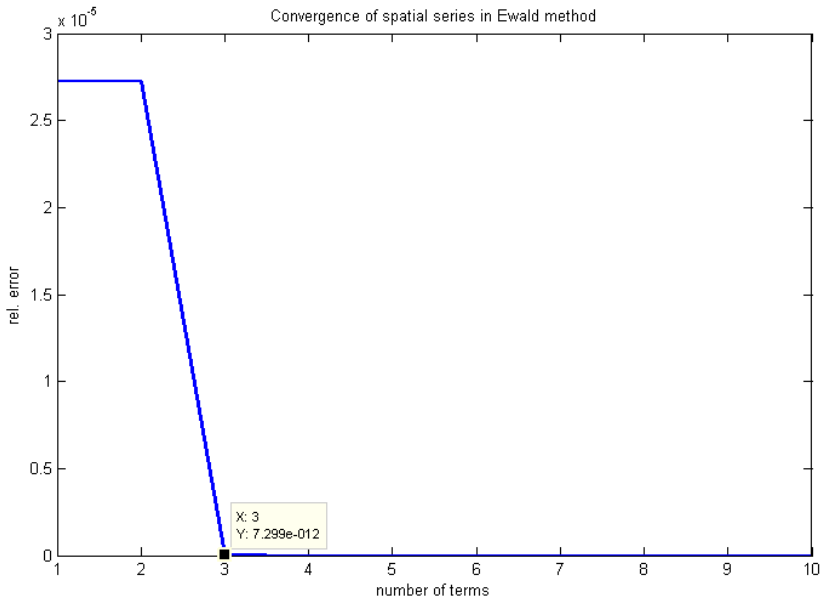

Figure 4.11: Convergence of the spatial series of Ewald summation for $a = b = 4.3\lambda_0$ and $E = E_{opt}$

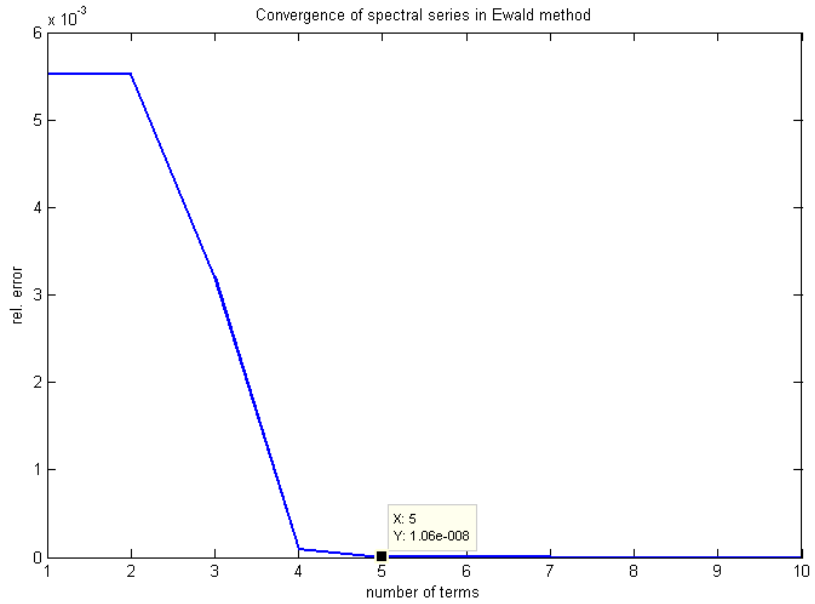

Figure 4.12: Convergence of the spectral series of Ewald summation for $a = b = 4.3\lambda_0$ and $E = 2E_{opt}$

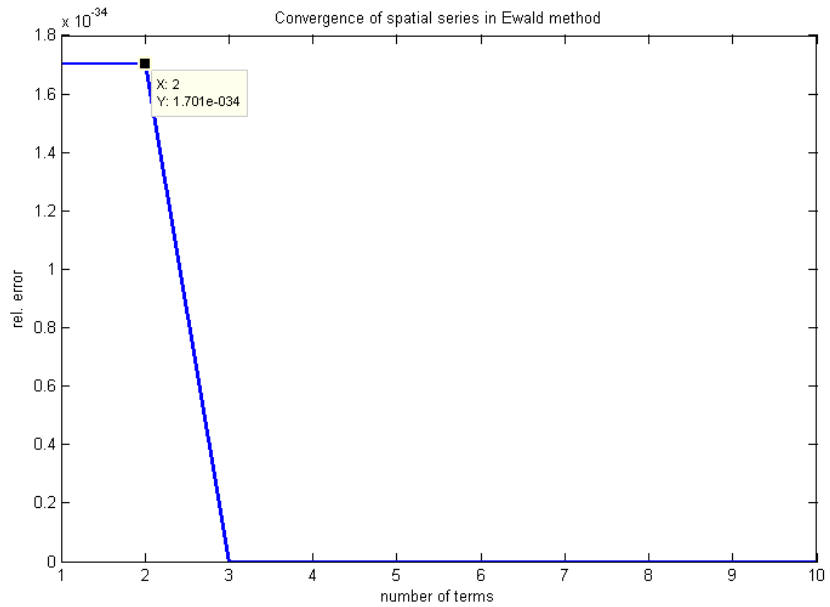

Figure 4.13: Convergence of the spatial series of Ewald summation for $a = b = 4.3\lambda_0$ and $E = 2E_{opt}$

a result, the total series converges to $5.685579541022889 + j9.017734101038668$. The new value for E solved the problem of accuracy loss which is due to the finite precision of the machine. However, this is accomplished at the cost of losing the optimum convergence rate for the series. This can be observed in Figures 4.12 and 4.13 in which the convergence of the spectral and the spatial series are shown, respectively.

The convergence rate of the spectral series has decreased while the convergence rate of the spatial series has increased with the choice of $E = 2E_{opt}$. The number of terms needed for the spectral series to converge is 11×11 while this number is 5×5 for the spatial series. This makes the total series converge more slowly compared to the case of $E = E_{opt}$ where the number of terms needed for both spectral and spatial series to converge is 7×7.

The results of this chapter show that the Ewald's method can successfully be applied to accelerate the series representing the periodic Green's function in multilayer media when this Green's function is approximated via DCIM.

CHAPTER 5

CONCLUSION AND THE FUTURE WORK

The aim of this thesis was to express the periodic Green's function in layered media in a suitable form such that the high order derivatives with respect to frequency can be easily obtained. For this purpose, the possibility of utilizing the DCIM is studied, 2-level and 3-level approximation schemes are applied. The numerical results show that there are mainly two factors that affect the accuracy of the method. First one is the contribution of surface wave poles; they need to be extracted before applying DCIM. Second one is the choice of the sampling path which is used to extract the parameters of the complex exponentials. The sampling path should be the real axis of the $k_\rho - plane$ since the Floquet mode summation of the periodic Green's function is also in terms of real values of k_ρ. By applying DCIM, the spectral domain Green's function is approximated in terms of two components which are the complex exponentials and the surface wave contributions.

After obtaining an accurate approximation for the spectral domain Green's function via DCIM, Ewald's method is used to compute the periodic Green's functions efficiently. It is demonstrated through numerical examples that the Floquet mode summations involved in the computation of the periodic Green's functions converge within a few terms (5 to 10) when Ewald's transformation is applied. However it should be noted that Ewald's transformation is applied only to the complex exponentials and the surface wave contributions are directly summed.

Although the main purpose of this thesis is achieved, the efficiency of the proposed method could be further improved by accelerating the series corresponding to surface wave contributions. This series could also be accelerated by applying Ewald's method. Because, in literature Ewald's method is utilized in the efficient computation of two dimensional free space periodic Green's function which involves Hankel functions and the surface wave contributions

are also in terms of Hankel functions. However, during the application of the Ewald's method to the series corresponding to the surface wave contributions, some numerical problems are encountered. The efforts to eliminate these problems are left as a future work.

As a future study it is also planned to use these accurate and efficient periodic Green's functions in the MoM analysis of periodic structures in layered media and to efficiently obtain the frequency response of such structures through the use of Pade approximation.

REFERENCES

[1] R. Gonzalo, P. de Maagt, M. Sorolla, ”Enhanced patch antenna performance by suppressing surface waves using photonic-bandgap substrates,” *IEEE Trans. Microwave Theory Tech.*, vol. 47, pp. 2131-2138, Nov. 1999.

[2] C. Cheype, M. Thevenot, R. T. Monodiere, A. Reineix, B. Jecko, ”An electromagnetic bandgap resonator antenna,” *IEEE Trans. Antennas Propag.*, vol. 50, pp. 1285-1290, Sep. 2002.

[3] W. J. Chappel, X. Gong, ”Wide bandgap composite EBG substrates,” *IEEE Trans. Antennas Propag.*, vol. 51, pp. 2744-2750, Oct. 2003.

[4] V. V. Varadan, ”Radar absorbing applications of metamaterials,” *IEEE Region 5 Technical Conference*, Apr. 2007.

[5] C. Qin, A. B. Kozyrev, A. Karbassi, D. W. van der Weide, ”Microfabricated V-band left-handed transmission lines,” *Metamaterials*, vol. 2, no. 1, pp. 26-35, May 2008.

[6] T. F. Eibert, J. L. Volakis, D. R. Wilton and D. R. Jackson, ”Hybrid FE/BI modeling of 3-D doubly periodic structures utilizing triangular prismatic elements and an MPIE formulation accelerated by the Ewald transformation,” *IEEE Trans. Antennas Propag.*, vol. 47, no. 5, pp. 843-850, May 1999.

[7] B. C. Usner, K. Sertel and J. L. Volakis, ”Doubly periodic volume-surface integral equation formulation for modeling metamaterials,” *IET Microwave Antennas Propag.*, vol. 1, no. 1, pp. 150-157, Feb. 2007.

[8] T. Güdü and L. Alatan, ”Use of asymptotic waveform evaluation technique in the analysis of multilayer structures with doubly periodic dielectric gratings,” *IEEE Trans. Antennas Propag.*, vol. 57, no. 9, pp. 2641-2649, Sep. 2009.

[9] F. Ling, D. Jiao and J. M. Jin, ”Efficient electromagnetic modeling of microstrip structures in multilayer media,” *IEEE Trans. Microwave Theory Tech.*, vol. 47, no. 9, pp. 1810-1818, Sep. 1999.

[10] R. M. Shubair and Y. L. Chow, ”Efficient computation of the periodic Green’s function in layered dielectric media,” *IEEE Trans. Microwave Theory Tech.*, vol. 41, no. 3, pp. 498-502, Mar. 1993.

[11] M. J. Park and S. Nam, ”Efficient calculation of the Green’s function for multilayered planar periodic structures,” *IEEE Trans. Antennas Propag.*, vol. 46, no. 10, pp. 1582-1583, Oct. 1998.

[12] D. Wang, E. K. N. Yung, R. S. Chen, D. Z. Ding and W. C. Tang, ”On evaluation of the Green function for periodic structures in layered media,” *IEEE Trans. Antennas Wireless Propag. Lett.*, vol. 3, pp. 133-136, 2004

[13] S. Singh, W. F. Richards, J. R. Zinecker, D. R. Wilton, "Accelerating the convergence of series representing the free space periodic Green's function," *IEEE Trans. Antennas Propag.*, vol. 38, no. 12, pp. 1958-1962, Dec. 1990.

[14] D. Shanks, "Non-linear transformations of divergent and slowly convergent sequences," *J. Math. Phys.*, vol. 34, pp. 1-42, 1955.

[15] N. Kınayman and M. I. Aksun, "Comparative study of acceleration techniques for integrals and series in electromagnetic problems," *Radio Science*, vol. 30, no. 6, pp. 1713-1722, Nov.-Dec. 1995.

[16] M. Abramowitz and I. A. Stegun, *Handbook of Mathematical Functions.* Dover, New York, 1965.

[17] N. Kinayman, M. I. Aksun, *Modern Microwave Circuits.* Artech House, London, 2005.

[18] R. W. Hamming, *Numerical Methods for Scientists and Engineers.* Dover, New York, 1973.

[19] Y. Hua and T. K. Sarkar, "Generalized pencil-of-function method for extracting poles of an EM system from its transient response," *IEEE Trans. Antennas Propag.*, vol. 37, no. 2, pp. 229-234, Feb. 1989.

[20] Y. L. Chow, "An approximate dynamic spatial Green's function in three dimensions for finite length microstrip lines," *IEEE Trans. Microwave Theory Tech.*, vol. MTT-28, pp. 393-397, 1980.

[21] Y. L. Chow, J. J. Yang, D. G. Fang and G. E. Howard, "A closed-form spatial Green's function for the thick microstrip substrate," *IEEE Trans. Microwave Theory Tech.*, vol. 39, pp. 588-592, Mar. 1991.

[22] E. Alanen and I. V. Lindell, "Exact image method for field calculation in horizontally layered medium above a conducting ground plane," *Proc. Inst. Elec. Eng.*, vol. 133, pt.H, pp. 297-304, 1986.

[23] D. G. Fang, J. J. Yang and G. Y. Delisle, "Discrete image theory for horizontal electric dipoles in a multilayered medium," *Proc. Inst. Elec. Eng.*, vol. 135, pt.H, pp. 297-303, 1988.

[24] M. I. Aksun, "A robust approach for the derivation of closed-form Green's functions," *IEEE Trans. Microwave Theory Tech.*, vol.44, no. 5, pp.651-658, May 1996.

[25] M. I. Aksun and G. Dural, "Clarification of issues on the closed-form Green's functions in stratified media," *IEEE Trans. Antennas Propag.*, vol. 53, no: 11, pp. 3644-3653, Nov. 2005.

[26] F. Mesa, R. R. Boix and F. Medina, "Closed-form expressions of multilayered planar Green's functions that account for the continuous spectrum in the far field," *IEEE Trans. Microwave Theory Tech.*, vol. 56, no. 7, pp. 1601-1614, Jul. 2008.

[27] A. Alparslan, M. I. Aksun and K. A. Michalski, "Closed-form Green's functions in planar layered media for all ranges and materials," *IEEE Trans. Microwave Theory Tech.*, vol. 58, no. 3, pp. 602-613, Mar. 2010.

[28] W. C. Chew, *Waves and Fields in Inhomogeneous Media.* Van Nostrand, New York, 1990.

[29] M. I. Aksun and R. Mittra, ”Derivation of closed-form Green’s functions for a general microstrip geometry,” *IEEE Trans. Microwave Theory Tech.*, vol. 40, no. 11, pp. 2055-2062, Nov. 1992.

[30] Constantine A. Balanis, *Advanced Engineering Electromagnetics.* Wiley, USA, 1989.

[31] F. Ling and J. M. Jin, ”Discrete complex image method for Green’s functions of general multilayer media,” *IEEE Trans. Microwave Guided Wave Lett.*, vol. 10, pp. 400-402, Oct. 2000.

[32] P. P. Ewald, ”Die berechnung optischer und electrostatischen gitterpotentiale,” *Ann. der Physik*, vol. 64, pp. 253-287, 1921. Translated by A. Cornell, Atomics International Library, 1964.

[33] K. E. Jordan, G. R. Richter and P. Sheng, ”An efficient numerical evaluation of the Green’s function for the Helmholtz operator on periodic structures,” *J. Comp. Phys.*, vol. 63, no. 1, pp. 222-235, Mar. 1986.

[34] F. Capolino, D. R. Wilton and W. A. Johnson, ”Efficient computation of the 2-D Green’s function for 1-D periodic structures using the Ewald method,” *IEEE Trans. Antennas Propag.*, vol. 53, no. 9, pp. 2977-2984, Sep. 2005.

[35] F. Capolino, D. R. Wilton and W. A. Johnson, ”Efficient computation of the 3D Green’s function for the Helmholtz operator for a linear array of point sources using the Ewald method,” *J. Comp. Phys.*, vol. 223, no. 1, pp. 250-261, Apr. 2007.

[36] D. R. Jackson, D. R. Wilton and N. J. Champagne, ”Efficient computation of periodic and nonperiodic Green’s function in layered media using the MPIE,” presented at the *URSI Int. Symp. Electrom. Theory*, Thessaloniki, Greece, May 25-28, 1998.

[37] M. J. Park, J. Park and S. Nam, ”Efficient calculation of the Green’s function for the rectangular cavity,” *IEEE Trans. Microwave Guided Wave Lett.*, vol. 8, no. 3, pp. 124-126, Mar. 1998.

[38] A. Kustepeli and A. Q. Martin, ”On the splitting parameter in the Ewald method,” *IEEE Trans. Microwave Guided Wave Lett.*, vol. 10, no. 5, pp. 168-170, May 2000.

[39] G. Dural and M. I. Aksun, ”Closed-form Green’s functions for general sources and stratified media,” *IEEE Trans. Microwave Theory Tech.*, vol. 43, pp. 1545-1552, July 1995.

[40] K. A. Michalski and J. R. Mosig, ”Multilayered media Green’s functions in integral equation formulations,” *IEEE Trans. Microwave Theory Tech.*, vol. 45, pp. 508-519, Mar. 1997.

[41] T. W. Gamelin, *Complex Analysis.* Springer, New York, 2001.

[42] Marcel Leutenegger, ”Error function of complex numbers,” *Ecole Polytechnique Federale de Lausanne (EPFL), Laboratoire d’Optique Biomedicale (LOB)*, Lausanne, Switzerland, 13 Jan. 2008.

[43] *http://www.mathworks.com/matlabcentral/fileexchange/18312-error-function-of-complex-numbers,* last accessed 30 Jan. 2011.

[44] M. J. Park and B. Lee, ”Efficient Calculation of the Green’s Function for 2-D Periodic Line Sources Using Ewald Method,” *IEEE Antennas Wireless Propag. Letters*, vol. 8, pp. 565-567, 2009.